Computers and Mathematics with Applications 114 (2022) 47–59

Contents lists available at ScienceDirect

Computers and Mathematics with Applications

www.elsevier.com/locate/camwa

A new numerical method for div-curl systems with low regularity assumptions

Shuhao Cao [a,1], Chunmei Wang [b,*,2], Junping Wang [c,3]

[a] Department of Mathematics and Statistics, Washington University in St. Louis, St. Louis, MO 63130, United States of America
[b] Department of Mathematics, University of Florida, Gainesville, FL 32611, United States of America
[c] Division of Mathematical Sciences, National Science Foundation, Alexandria, VA 22314, United States of America

ARTICLE INFO

Dataset link: https://doi.org/10.24433/CO.4347043.v1

Keywords:
Finite element methods
Weak Galerkin methods
Primal-dual weak Galerkin
Div-curl system

ABSTRACT

This paper presents a new numerical method for div-curl systems with the normal boundary condition by using a finite element technique known as primal-dual weak Galerkin (PDWG). The PDWG finite element scheme for the div-curl system has two prominent features in that it offers not only an accurate and reliable numerical solution to the div-curl system under the low H^{α}-regularity ($\alpha > 0$) assumption for the true solution, but also an effective approximation of the normal harmonic vector fields on domains with complex topology. Seven numerical experiments are conducted and the results are presented to demonstrate the performance of the PDWG algorithm, including one example on the computation of discrete normal harmonic vector fields.

1. Introduction

In this paper we are concerned with the development of new numerical methods for div-curl systems equipped with normal boundary conditions. For simplicity, consider the model problem that seeks a vector field $\boldsymbol{u} = \boldsymbol{u}(\boldsymbol{x})$ satisfying

$$\nabla \cdot (\varepsilon \boldsymbol{u}) = f, \quad \text{in } \Omega, \tag{1.1}$$

$$\nabla \times \boldsymbol{u} = \boldsymbol{g}, \quad \text{in } \Omega, \tag{1.2}$$

$$\varepsilon \boldsymbol{u} \cdot \boldsymbol{n} = \phi_1, \quad \text{on } \Gamma, \tag{1.3}$$

where $\Omega \subset \mathbb{R}^3$ is an open, bounded and connected polyhedral domain. $\Gamma = \partial\Omega$ is the boundary of Ω. Assume that the domain boundary is the union of a finite number of disjoint surfaces $\Gamma = \bigcup_{i=0}^{L} \Gamma_i$, where Γ_0 is the exterior boundary of Ω, Γ_i $(i = 1, \cdots, L)$ are the other connected components with finite surface areas. The load function $f = f(\boldsymbol{x})$ and the vector field $\boldsymbol{g} = \boldsymbol{g}(\boldsymbol{x})$ are given in the domain Ω, the coefficient matrix $\varepsilon = \{\varepsilon_{ij}(\boldsymbol{x})\}_{3\times 3}$ is assumed to be symmetric and uniformly positive definite in Ω, and the entries ε_{ij} $(i, j = 1, 2, 3)$ are in $L^{\infty}(\Omega)$. The normal boundary data ϕ_1 is a given function in $H^{-\frac{1}{2}}(\Gamma)$.

The solution uniqueness for the normal boundary value problem (1.1)-(1.3) depends on the topology of the domain Ω. It is well-known that the solution uniqueness holds true for simply connected Ω, while the solution is unique up to a normal ε-harmonic function in $\mathbb{H}_{\varepsilon n,0}(\Omega)$ defined in (2.2) when the domain Ω is not simply connected. The dimension of $\mathbb{H}_{\varepsilon n,0}(\Omega)$ is identical to the first Betti number of Ω, which is the rank of the first homology group of Ω.

The div-curl system (1.1)-(1.2) arises in many applications such as electromagnetic fields and fluid mechanics. Computational electromagnetics plays an important role in many areas of science and engineering such as radar, satellite, antenna design, waveguides, optical fibers, medical imaging and design of invisible cloaking devices [15]. In linear magnetic fields, the function $f(\boldsymbol{x})$ vanishes, $\boldsymbol{u}$ represents the magnetic field intensity and $\varepsilon(\boldsymbol{x})$ is the inverse of the magnetic permeability tensor. In fluid mechanics fields, the coefficient matrix $\varepsilon(\boldsymbol{x})$ is diagonal with diagonal entries being the local mass density. In electrostatics fields, $\varepsilon(\boldsymbol{x})$ is the permittivity matrix.

The code (and data) in this article has been certified as Reproducible by Code Ocean: https://codeocean.com/. More information on the Reproducibility Badge Initiative is available at https://www.elsevier.com/physical-sciences-and-engineering/computer-science/journals.

* Corresponding author.
E-mail addresses: s.cao@wustl.edu (S. Cao), chunmei.wang@ufl.edu (C. Wang), jwang@nsf.gov (J. Wang).

[1] The research of Shuhao Cao was partially supported by National Science Foundation Award DMS-1913080.
[2] The research of Chunmei Wang was partially supported by National Science Foundation Award DMS-2136380.
[3] The research of Junping Wang was supported by the NSF IR/D program, while working at National Science Foundation. However, any opinion, finding, and conclusions or recommendations expressed in this material are those of the author and do not necessarily reflect the views of the National Science Foundation.

https://doi.org/10.1016/j.camwa.2022.03.015
Received 1 June 2021; Received in revised form 7 February 2022; Accepted 5 March 2022
Available online 30 March 2022

Several numerical methods based on finite element approaches have been proposed and analyzed for the div-curl system (1.1)-(1.2). Bossavit [3] proposed a classical numerical method for solving the magnetostatic problem by introducing a scalar or vector potential. A covolume method was developed in three dimensional space by using the Voronoi-Delaunay mesh pairs [20]. The control volume method [19] was proposed directly for planar div-curl problems. A discrete duality finite volume method [9] was presented for div-curl problems on almost arbitrary polygonal meshes. In [4,17], the authors introduced a mimetic finite difference scheme for the three dimensional magneto-static problems on general polyhedral partitions, which has a closer connection with the discretization schemes to be presented than any other existing methods in literature. The numerical algorithm [21] was designed for constructing a finite element basis for the first de Rham cohomology group of the computational domain, which was further used for a numerical approximation of the magnetostatic problem. In [8], the authors developed a mixed finite element method for three dimensional axisymmetric div-curl systems through a dimension reduction technique based on the cylindrical coordinates in simply connected and axisymmetric domains. In [2], the authors developed a least-squares finite element method for two types boundary value problems. Another least-squares method was proposed for the div-curl problem based on discontinuous elements on nonconvex polyhedral domains in [1]. In [23], the authors proposed a weak Galerkin finite element method for the div-curl system with either normal or tangential boundary conditions. Another weak Galerkin scheme was introduced in [16] by using a least-squares approach for the div-curl problem. In [18], the authors developed a primal-dual weak Galerkin finite element method for the div-curl system with tangential boundary conditions and proved that the scheme works well with low-regularity assumptions on the exact solution.

There are two main challenges in the approximation of the div-curl system (1.1)-(1.3): (1) the low-regularity of the true solution $\boldsymbol{u}$ which limits the stability and accuracy of the numerical solutions, and (2) the non-uniqueness of the solution $\boldsymbol{u}$ on domains with complex topology. In particular, for domains with positive first Betti number, the Helmholtz decomposition in Theorem A.1 involves a nontrivial space of harmonic field $\mathbb{H}_{\varepsilon n,0}(\Omega)$ so that the solution to the div-curl system (1.1)-(1.3) is non-unique. The second challenge can be relaxed to certain extent by seeking a particular solution orthogonal to the space of normal ε-harmonic vector space $\mathbb{H}_{\varepsilon n,0}(\Omega)$, but with an immediate obstacle lying in the determination of the space $\mathbb{H}_{\varepsilon n,0}(\Omega)$ or an effective approximation of this space. To address these challenges, we shall devise a new primal-dual weak Galerkin (PDWG) scheme for (1.1)-(1.3) by following the framework developed in [18] for the div-curl system with tangential boundary conditions. The difference between the present work and [18] lies in the second challenge (i.e., the solution non-uniqueness) for which the tangential boundary value problem does not have, and hence, less difficulty was encountered in [18]. For problems with non-unique solutions, good numerical methods must be able to inform the computational practitioners about where and how the numerical solutions are converging to. Our new PDWG scheme will do exactly this job for the model div-curl problem (1.1)-(1.3). It should be noted that the PDWG framework was originated in [25] and further developed in [22,27,28,5,24,14,26] for several other model problems. A similar numerical method, known as *stabilized finite element methods*, was devised by Burman in a different context [11,12,10].

Our PDWG numerical method for (1.1)-(1.3) has two prominent features over the existing numerical methods: (1) it offers an effective approximation of the normal ε-harmonic vector space $\mathbb{H}_{\varepsilon n,0}(\Omega)$ regardless of the topology of the domain Ω (see Example 7 for an illustration); and (2) it provides an accurate and reliable numerical solution for the div-curl system (1.1)-(1.3) with low H^{α}-regularity ($\alpha > 0$) assumption for the true solution $\boldsymbol{u}$.

The paper is organized as follows. Section 2 is devoted to notations and the derivation of a weak formulation for the div-curl system (1.1)-(1.3) that involves no partial derivatives over the vector field $\boldsymbol{u}$. Section 3 offers a brief review on the discrete weak gradient and discrete weak curl operators. Section 4 is dedicated to the presentation of the PDWG algorithm for the div-curl problem, together with an algorithm for computing discrete normal ε-harmonic vector fields. Section 5 is devoted to a discussion of the solution existence and uniqueness for the PDWG scheme. Section 6 contains a convergence theory for the PDWG approximation, and Section 7 demonstrates the performance of the PDWG algorithm through seven test examples.

2. Notations and preliminaries

We follow the usual notation for Sobolev spaces and norms, see for example [7,13]. For an open bounded domain $D \subset \mathbb{R}^3$ with Lipschitz continuous boundary and any given real number $s \geq 0$, we use $\|\cdot\|_{s,D}$ and $|\cdot|_{s,D}$ to denote the norm and seminorm in the Sobolev space $H^s(D)$, respectively. The space $H^0(D)$ coincides with $L^2(D)$, for which the norm and the inner product are denoted by $\|\cdot\|_D$ and $(\cdot,\cdot)_D$, respectively. We use $H(div_\varepsilon; D)$ to denote the closed subspace of $[L^2(D)]^2$ so that $\nabla\cdot(\varepsilon\boldsymbol{v}) \in L^2(D)$. The space $H(div; D)$ corresponds to the case of $\varepsilon = I$. Analogously, we use $H(curl; D)$ to denote the closed subspace of $[L^2(D)]^2$ so that $\nabla\times\boldsymbol{v} \in [L^2(D)]^3$. Denote by

$$H_0(curl; D) := \{\boldsymbol{v} \in H(curl; D),\ \boldsymbol{v}\times\boldsymbol{n} = 0 \text{ on } \partial D\}$$

the closed subspace with vanishing tangential boundary values. When $D = \Omega$, we shall drop the script D in the notations. For simplicity, we shall denote by $\langle\cdot,\cdot\rangle_{\Gamma_i}$ the inner product in $L^2(\Gamma_i)$ and use "$\lesssim$" to denote "less than or equal to up to a general constant independent of the mesh size or functions appearing in the inequality".

Introduce the following Sobolev space

$$\mathbb{W}_\varepsilon(\Omega) = \{\boldsymbol{v} \in H_0(curl) \cap H(div_\varepsilon),\ \nabla\cdot(\varepsilon\boldsymbol{v}) = 0,\ \langle\varepsilon\boldsymbol{v}\cdot\boldsymbol{n}_i, 1\rangle_{\Gamma_i} = 0,\ i = 1,\cdots,L\}. \tag{2.1}$$

A vector field $\boldsymbol{v} \in [L^2(\Omega)]^3$ is said to be ε-harmonic on Ω if it is ε-solenoidal and irrotational on Ω. The space of normal ε-harmonic vector fields, denoted by $\mathbb{H}_{\varepsilon n,0}(\Omega)$, consists of all ε-harmonic vector fields satisfying the zero normal boundary condition; i.e.,

$$\mathbb{H}_{\varepsilon n,0}(\Omega) = \{\boldsymbol{v} \in [L^2(\Omega)]^3 :\ \nabla\times\boldsymbol{v} = 0,\ \nabla\cdot(\varepsilon\boldsymbol{v}) = 0,\ \varepsilon\boldsymbol{v}\cdot\boldsymbol{n} = 0 \text{ on } \Gamma\}. \tag{2.2}$$

When $\varepsilon = I$ is the identity matrix, the space $\mathbb{H}_{\varepsilon n,0}(\Omega)$ shall be denoted as $\mathbb{H}_{n,0}(\Omega)$. Analogously, the space of tangential ε-harmonic vector fields, denoted by $\mathbb{H}_{\varepsilon\tau,0}(\Omega)$, consists of all ε-harmonic vector fields satisfying the zero tangential boundary condition; i.e.,

$$\mathbb{H}_{\varepsilon\tau,0}(\Omega) = \{\boldsymbol{v} \in [L^2(\Omega)]^3 :\ \nabla\times\boldsymbol{v} = 0,\ \nabla\cdot(\varepsilon\boldsymbol{v}) = 0,\ \boldsymbol{v}\times\boldsymbol{n} = 0 \text{ on } \Gamma\}.$$

2.1. A weak formulation

By testing the equation (1.1) against any $\varphi \in H^1(\Omega)$ and then using the normal boundary condition (1.3) we obtain

$$(\boldsymbol{u}, \varepsilon\nabla\varphi) = \langle\phi_1, \varphi\rangle - (f, \varphi), \qquad \forall\varphi \in H^1(\Omega). \tag{2.3}$$

Next, we test the equation (1.2) against any $\boldsymbol{w} \in H_0(curl;\Omega)$ to obtain

$$(\boldsymbol{u}, \nabla\times\boldsymbol{w}) = (\boldsymbol{g}, \boldsymbol{w}), \qquad \forall\boldsymbol{w} \in H_0(curl;\Omega). \tag{2.4}$$

Summing the equations (2.3) and (2.4) gives the following

$$(\boldsymbol{u}, \varepsilon\nabla\varphi + \nabla\times\boldsymbol{w}) = (\boldsymbol{g}, \boldsymbol{w}) - (f, \varphi) + \langle\phi_1, \varphi\rangle$$

for all $\varphi \in H^1(\Omega)$ and $\boldsymbol{w} \in H_0(curl;\Omega)$.

Definition 2.1. A vector-valued function $\boldsymbol{u} \in [L^2(\Omega)]^3$ is said to be a weak solution of the normal boundary value problem for the div-curl system (1.1)-(1.3) if it satisfies the following equation

$$(\boldsymbol{u}, \varepsilon\nabla\varphi + \nabla\times\boldsymbol{\psi}) = (\boldsymbol{g}, \boldsymbol{\psi}) - (f, \varphi) + \langle\phi_1, \varphi\rangle \tag{2.5}$$

for all $\varphi \in H^1(\Omega)$ and $\boldsymbol{\psi} \in H_0(curl;\Omega)$.

The solution to the variational problem (2.5) is generally non-unique. In fact, the homogeneous version of (2.5) seeks $\boldsymbol{u} \in [L^2(\Omega)]^3$ satisfying

$$(\boldsymbol{u}, \varepsilon\nabla\varphi + \nabla\times\boldsymbol{\psi}) = 0 \qquad \forall\varphi \in H^1(\Omega),\ \boldsymbol{\psi} \in H_0(curl;\Omega). \tag{2.6}$$

The equation (2.6) is easily satisfied by any ε-harmonic function $\boldsymbol{u} = \boldsymbol{\eta} \in \mathbb{H}_{\varepsilon n,0}(\Omega)$, and hence the solution non-uniqueness when the ε-harmonic space $\mathbb{H}_{\varepsilon n,0}(\Omega)$ has a positive dimension. The solution to the div-curl system with normal boundary condition is unique when the solution is further required to be ε-weighted L^2 orthogonal to $\mathbb{H}_{\varepsilon n,0}(\Omega)$.

2.2. An extended weak formulation

Denote by $H^1_{0c}(\Omega)$ the space of functions in $H^1(\Omega)$ with vanishing value on Γ_0 and constant values on other connected components of the boundary; i.e.,

$$H^1_{0c}(\Omega) = \{\phi \in H^1(\Omega) :\ \phi|_{\Gamma_0} = 0,\ \phi|_{\Gamma_i} = \alpha_i,\ i = 1,\dots,L\}.$$

Introduce the following bilinear form:

$$B(\boldsymbol{u}, s; \varphi, \boldsymbol{\psi}) := (\boldsymbol{u}, \varepsilon\nabla\varphi + \nabla\times\boldsymbol{\psi}) + (\boldsymbol{\psi}, \varepsilon\nabla s). \tag{2.7}$$

The extended weak formulation for the normal boundary value problem of the div-curl system seeks $(\boldsymbol{u}, s) \in [L^2(\Omega)]^3 \times H^1_{0c}(\Omega)$ such that

$$B(\boldsymbol{u}, s; \varphi, \boldsymbol{\psi}) = F(\varphi, \boldsymbol{\psi}) \qquad \forall\varphi \in H^1(\Omega), \forall\boldsymbol{\psi} \in H_0(curl;\Omega), \tag{2.8}$$

where

$$F(\varphi, \boldsymbol{\psi}) = (\boldsymbol{g}, \boldsymbol{\psi}) - (f, \varphi) + \langle\phi_1, \varphi\rangle.$$

Note that by testing the curl equation in the div-curl system against any $\rho \in H^1_{0c}(\Omega)$ we have

$$(\boldsymbol{g}, \nabla\rho) = 0, \qquad \forall\rho \in H^1_{0c}(\Omega), \tag{2.9}$$

which gives rise to the following compatibility condition:

$$\nabla\cdot\boldsymbol{g} = 0, \quad \langle\boldsymbol{g}\cdot\boldsymbol{n}_i, 1\rangle_{\Gamma_i} = 0, \text{ for } i = 1,\cdots,L. \tag{2.10}$$

Theorem 2.1. *Under the compatibility condition (2.10) for $\boldsymbol{g}$, the solution $(\boldsymbol{u}; s)$ of (2.8) satisfies the following equations:*

$$\nabla\cdot(\varepsilon\boldsymbol{u}) = f, \qquad \text{in } \Omega, \tag{2.11}$$

$$\nabla\times\boldsymbol{u} = \boldsymbol{g}, \qquad \text{in } \Omega, \tag{2.12}$$

$$s = 0, \qquad \text{in } \Omega, \tag{2.13}$$

$$\varepsilon\boldsymbol{u}\cdot\boldsymbol{n} = \phi_1, \qquad \text{on } \Gamma. \tag{2.14}$$

Proof. By letting $\boldsymbol{\psi} = 0$ in (2.8) we have

$$(\boldsymbol{u}, \varepsilon\nabla\varphi) = -(f, \varphi) + \langle\phi_1, \varphi\rangle_\Gamma$$

for all $\varphi \in H^1(\Omega)$. It follows that $\nabla\cdot(\varepsilon\boldsymbol{u}) = f$ and $\varepsilon\boldsymbol{u}\cdot\boldsymbol{n} = \phi_1$ on Γ, which leads to (2.11) and (2.14). Next, by letting $\varphi = 0$ in (2.8) we arrive at

$$(\boldsymbol{u}, \nabla\times\boldsymbol{\psi}) + (\boldsymbol{\psi}, \varepsilon\nabla s) = (\boldsymbol{g}, \boldsymbol{\psi}), \qquad \forall\boldsymbol{\psi} \in H_0(curl;\Omega),$$

which leads to

$$(\nabla\times\boldsymbol{u} + \varepsilon\nabla s, \boldsymbol{\psi}) = (\boldsymbol{g}, \boldsymbol{\psi}),$$

and thus

$$\nabla\times\boldsymbol{u} + \varepsilon\nabla s = \boldsymbol{g}, \qquad \text{in } \Omega. \tag{2.15}$$

Now from (2.15) we have

$$(\nabla\times\boldsymbol{u} + \varepsilon\nabla s, \nabla s) = (\boldsymbol{g}, \nabla s),$$

which, by the usual integration by parts, gives

$$\langle\boldsymbol{n}\times\boldsymbol{u}, \nabla s\rangle_\Gamma + (\varepsilon\nabla s, \nabla s) = (\boldsymbol{g}, \nabla s),$$

and by the boundary condition of $s = const$ on each Γ_i and the compatibility condition (2.10)

$$(\varepsilon\nabla s, \nabla s) = \langle\boldsymbol{u}, \boldsymbol{n}\times\nabla s\rangle_\Gamma + (\boldsymbol{g}, \nabla s) = 0.$$

It follows that $\nabla s = 0$ so that $s \equiv 0$. This completes the proof of the theorem. □

The homogeneous dual problem of (2.8) seeks $\lambda \in H^1(\Omega)/\mathbb{R}$ and $\boldsymbol{q} \in H_0(curl;\Omega)$ satisfying

$$B(\boldsymbol{v}, r; \lambda, \boldsymbol{q}) = 0 \qquad \forall\boldsymbol{v} \in [L^2(\Omega)]^3,\ r \in H^1_{0c}(\Omega). \tag{2.16}$$

Theorem 2.2. *The solution to the homogeneous dual problem (2.16) is unique.*

Proof. The problem (2.16) can be rewritten as

$$(\boldsymbol{v}, \varepsilon\nabla\lambda + \nabla\times\boldsymbol{q}) + (\boldsymbol{q}, \varepsilon\nabla r) = 0 \tag{2.17}$$

for all $\boldsymbol{v} \in [L^2(\Omega)]^3$ and $r \in H^1_{0c}(\Omega)$. Note that the test against $r \in H^1_{0c}(\Omega)$ and $\boldsymbol{v} = 0$ ensures $\nabla\cdot(\varepsilon\boldsymbol{q}) = 0$ and $\langle\varepsilon\boldsymbol{q}\cdot\boldsymbol{n}, 1\rangle_{\Gamma_i} = 0$ for all $i \in \{1,\cdots,L\}$. In addition, by letting $r = 0$ and varying $\boldsymbol{v} \in [L^2(\Omega)]^3$ we arrive at

$$\varepsilon\nabla\lambda + \nabla\times\boldsymbol{q} = 0,$$

which, by testing against $\nabla\lambda$, leads to

$$(\varepsilon\nabla\lambda, \nabla\lambda) = 0,$$

so that $\lambda \equiv 0$ and hence

$$\nabla\times\boldsymbol{q} = 0.$$

Thus, we have

$$\boldsymbol{q} \in \mathbb{H}_{\varepsilon\tau,0}(\Omega), \quad \langle\varepsilon\boldsymbol{q}\cdot\boldsymbol{n}_i, 1\rangle_{\Gamma_i} = 0 \text{ for } i = 1,\cdots,L,$$

which yields $\boldsymbol{q} \equiv 0$. □

3. Discrete weak gradient and weak curl

The extended weak formulation (2.8) is based on the gradient and curl differential operators. In this section, we shall review the notion of discrete weak gradient and weak curl which forms a corner stone of the weak Galerkin finite element method. To this end, let T be a polyhedral domain with boundary ∂T and unit outward normal direction $\boldsymbol{n}$ on ∂T. Define the space of weak functions in T by

$$W(T) = \{v = \{v_0, v_b\} : v_0 \in L_2(T), v_b \in L_2(\partial T)\},$$

where v_0 represents the value of v in the interior of T, and v_b represents some specific boundary information of v. Analogously, define the space of vector-valued weak functions on T by

$$V(T) = \{\boldsymbol{v} = \{\boldsymbol{v}_0, \boldsymbol{v}_b\} : \boldsymbol{v}_0 \in [L_2(T)]^3, \boldsymbol{v}_b \in [L_2(\partial T)]^3\}.$$

Let $P_j(T)$ the space of polynomials on T with total degree j and less. For any $v \in W(T)$, the discrete weak gradient, denoted by $\nabla_{w,j,T}v$, is defined as the unique vector-valued polynomial in $[P_j(T)]^3$ satisfying

$$(\nabla_{w,j,T}v, \boldsymbol{\varphi})_T = -(v_0, \nabla\cdot\boldsymbol{\varphi})_T + \langle v_b, \boldsymbol{\varphi}\cdot\boldsymbol{n}\rangle_{\partial T}, \quad \forall\,\boldsymbol{\varphi} \in [P_j(T)]^3. \tag{3.1}$$

Analogously, the discrete weak curl of $\boldsymbol{v} \in V(T)$, denoted by $\nabla_{w,j,T}\times\boldsymbol{v}$, is defined as the unique vector-valued polynomial in $[P_j(T)]^3$, satisfying

$$(\nabla_{w,j,T}\times\boldsymbol{v}, \boldsymbol{\varphi})_T = (\boldsymbol{v}_0, \nabla\times\boldsymbol{\varphi})_T - \langle\boldsymbol{v}_b\times\boldsymbol{n}, \boldsymbol{\varphi}\rangle_{\partial T}, \quad \forall\,\boldsymbol{\varphi} \in [P_j(T)]^3. \tag{3.2}$$

4. PDWG numerical algorithm

Let $\mathcal{T}_h$ be a finite element partition of the domain Ω consisting of polyhedra that are shape-regular [29]. Denote by $\mathcal{E}_h$ the set of faces in $\mathcal{T}_h$ and $\mathcal{E}_h^0 = \mathcal{E}_h \setminus \partial\Omega$ the set of interior faces. Denote by h_T the diameter of the element $T \in \mathcal{T}_h$ and $h = \max_{T\in\mathcal{T}_h} h_T$ the meshsize of the partition $\mathcal{T}_h$.

For a given integer $k \geq 0$, we introduce the following finite element spaces subordinated to $\mathcal{T}_h$:

$$\boldsymbol{V}_h = \{\boldsymbol{v} : \ \boldsymbol{v}|_T \in [P_k(T)]^3, \forall T \in \mathcal{T}_h\},$$

$$S_h = \{\{s_0, s_b\} : \ s_0|_T \in P_k(T), s_b|_{\partial T} \in P_k(\partial T), \forall T \in \mathcal{T}_h, s_b|_{\Gamma_0} = 0, \ s_b|_{\Gamma_i} \text{ is a constant}\},$$

$$M_h = \{\{\varphi_0, \varphi_b\} : \ \varphi_0|_T \in P_k(T), \varphi_b|_{\partial T} \in P_k(\partial T), \forall T \in \mathcal{T}_h, \int_\Omega \varphi_0 = 0\},$$

$$\boldsymbol{W}_h = \{\boldsymbol{\psi} = \{\boldsymbol{\psi}_0, \boldsymbol{\psi}_b\} : \ \boldsymbol{\psi}_0|_T \in [P_k(T)]^3, \boldsymbol{\psi}_b|_{\partial T} \in G_k(\partial T), \forall T \in \mathcal{T}_h, \ \boldsymbol{\psi}_b|_\Gamma = 0\},$$

where $G_k(\partial T) := [P_k(\sigma)]^3 \times \boldsymbol{n}_\sigma$ is the space of polynomials of degree k in the tangent space of ∂T.

For simplicity of notation, for $\sigma \in S_h$ or $\sigma \in M_h$, denote by $\nabla_w \sigma$ the discrete weak gradient $\nabla_{w,k,T}\sigma$ computed by using (3.1) on each element T; i.e.,

$$(\nabla_w \sigma)|_T = \nabla_{w,k,T}(\sigma|_T), \qquad \sigma \in S_h \text{ or } \sigma \in M_h.$$

Analogously, for $\boldsymbol{q} \in \boldsymbol{W}_h$, denote by $\nabla_w \times \boldsymbol{q}$ the discrete weak curl $\nabla_{w,k,T} \times \boldsymbol{q}$ computed by using (3.2) on each element T; i.e.,

$$(\nabla_w \times \boldsymbol{q})|_T = \nabla_{w,k,T} \times (\boldsymbol{q}|_T), \qquad \boldsymbol{q} \in \boldsymbol{W}_h.$$

An approximation of the bilinear form $B(\cdot;\cdot)$ is given as follows:

$$B_h(\boldsymbol{u}_h, s_h; \varphi, \boldsymbol{\psi}) := (\boldsymbol{u}_h, \varepsilon\nabla_w\varphi + \nabla_w \times \boldsymbol{\psi}) + (\boldsymbol{\psi}_0, \varepsilon\nabla_w s_h) \tag{4.1}$$

for $\boldsymbol{u}_h \in \boldsymbol{V}_h$, $s_h \in S_h$, $\varphi \in M_h$, $\boldsymbol{\psi} \in \boldsymbol{W}_h$.

The following is the PDWG finite element method for the div-curl model system (1.1)-(1.3).

Algorithm 1 *(PDWG Algorithm).* For an approximate solution of (1.1)-(1.3), one may compute $\boldsymbol{u}_h \in \boldsymbol{V}_h$, together with three auxiliary variables $s_h \in S_h$, $\lambda_h \in M_h$, and $\boldsymbol{q}_h \in \boldsymbol{W}_h$ satisfying

$$\begin{cases} s_1(\lambda_h, \boldsymbol{q}_h; \varphi, \boldsymbol{\psi}) + B_h(\boldsymbol{u}_h, s_h; \varphi, \boldsymbol{\psi}) &= F(\varphi, \boldsymbol{\psi}), \quad \forall \varphi \in M_h, \ \boldsymbol{\psi} \in \boldsymbol{W}_h, \\ -s_2(s_h, r) + B_h(\boldsymbol{v}, r; \lambda_h, \boldsymbol{q}_h) &= 0, \quad \forall \boldsymbol{v} \in \boldsymbol{V}_h, \ r \in S_h. \end{cases} \tag{4.2}$$

Here the stabilizer s_1 is given by

$$s_1(\lambda_h, \boldsymbol{q}_h; \varphi, \boldsymbol{\psi}) = \rho_1 \sum_{T\in\mathcal{T}_h} h_T^{-1} \langle \lambda_0 - \lambda_b, \varphi_0 - \varphi_b \rangle_{\partial T} + \rho_2 \sum_{T\in\mathcal{T}_h} h_T^{-1} \langle \boldsymbol{q}_0 \times \boldsymbol{n} - \boldsymbol{q}_b \times \boldsymbol{n}, \boldsymbol{\psi}_0 \times \boldsymbol{n} - \boldsymbol{\psi}_b \times \boldsymbol{n} \rangle_{\partial T}, \tag{4.3}$$

and s_2 is defined accordingly in the space M_h as follows

$$s_2(s_h; r) = \rho_3 \sum_{T\in\mathcal{T}_h} h_T^{-\gamma} \langle s_0 - s_b, r_0 - r_b \rangle_{\partial T},$$

where $\gamma \geq -1$ and $\rho_i > 0$ are parameters with values at user's discretion.

The PDWG scheme (4.2) further provides an approximation of the space of normal ε-harmonic vector fields $\mathbb{H}_{\varepsilon n,0}(\Omega)$, as revealed by Theorem 6.2 in that the difference $\boldsymbol{\eta}_h = Q_h\boldsymbol{u} - \boldsymbol{u}_h$ is sufficiently close to a true normal ε-harmonic vector field $\boldsymbol{\eta}$. For this purpose, we introduce the following notation of discrete normal ε-harmonic functions.

Definition 4.1 *(discrete normal ε-harmonic functions).* A vector field $\boldsymbol{\eta}_h \in \boldsymbol{V}_h$ is said to be a discrete normal ε-harmonic function if there exists a vector field $\boldsymbol{u} \in H(div_\varepsilon; \Omega) \cap H(curl; \Omega)$ such that

$$\boldsymbol{\eta}_h = Q_h\boldsymbol{u} - \boldsymbol{u}_h, \tag{4.4}$$

where Q_h is the L^2 projection operator onto the finite element space $\boldsymbol{V}_h$ and $\boldsymbol{u}_h$ is the solution of (4.2) for a div-curl system (1.1)-(1.3) with load functions f, $\boldsymbol{g}$, and ϕ_1 determined by $\boldsymbol{u}$.

In practical computation, a discrete normal ε-harmonic function can be readily obtained from (4.4) by choosing a smooth vector field $\boldsymbol{u}$ and one solving of the PDWG system (4.2).

5. Solution existence and uniqueness

Introduce two semi-norms as follows:

$$|||(\lambda_h, \boldsymbol{q}_h)||| = \Big(s_1(\lambda_h, \boldsymbol{q}_h; \lambda_h, \boldsymbol{q}_h)\Big)^{\frac{1}{2}}, \qquad \lambda_h \in M_h, \ \boldsymbol{q}_h \in \boldsymbol{W}_h, \tag{5.1}$$

$$|||s_h||| = \Big(s_2(s_h; s_h)\Big)^{\frac{1}{2}}, \qquad s_h \in S_h. \tag{5.2}$$

For simplicity, assume that ε is piecewise constant with respect to the partition $\mathcal{T}_h$. Note that all the results can be generalized to piecewise smooth ε without any difficulty.

Denote by Q_0 the L^2 projection operator onto $P_k(T)$ and Q_b the L^2 projection operator onto $P_k(\sigma)$ on each face $\sigma \in \partial T$. Denote by Q_h the projection operator onto the weak finite element space S_h or M_h such that

$$(Q_h w)|_T = \{Q_0 w|_T, Q_b w|_{\partial T}\}.$$

Analogously, we use $\mathbb{Q}_0$, $\mathbb{Q}_b$ and $\mathbb{Q}_h$ to denote the L^2 projection operators onto $[P_k(T)]^3$, $G_k(\sigma) = [P_k(\sigma)]^3 \times \boldsymbol{n}_\sigma$, and $\boldsymbol{W}_h$, respectively. The L^2 projection operator onto the finite element space $\boldsymbol{V}_h$ is denoted as $\mathcal{Q}_h$.

Lemma 5.1. *[29] The L^2 projections Q_h and $\mathcal{Q}_h$ satisfy the commutative property*

$$\nabla_w(Q_h w) = \mathcal{Q}_h(\nabla w), \qquad \forall w \in H^1(T), \tag{5.3}$$

$$\nabla_w \times (\mathbb{Q}_h \boldsymbol{\psi}) = \mathcal{Q}_h(\nabla \times \boldsymbol{\psi}), \qquad \forall \boldsymbol{\psi} \in H(curl; T). \tag{5.4}$$

Theorem 5.2. *The kernel of the matrix of the PDWG finite element scheme (4.2) is given by*

$$K_h = \{(\boldsymbol{v}_h, s_h = 0, \lambda_h = 0, \boldsymbol{q}_h = 0) : \ \boldsymbol{v}_h \in \boldsymbol{V}_h \cap \mathbb{H}_{\varepsilon n,0}(\Omega)\}.$$

In other words, the kernel of the matrix of the PDWG scheme (4.2) is isomorphic to the subspace of $\mathbb{H}_{\varepsilon n,0}(\Omega)$ consisting of harmonic functions that are piecewise polynomial of degree k.

Proof. Let $(\boldsymbol{u}_h, s_h, \lambda_h, \boldsymbol{q}_h)$ be a solution of (4.2) with homogeneous data. It follows that

$$s_1(\lambda_h, \boldsymbol{q}_h; \lambda_h, \boldsymbol{q}_h) = 0, \quad s_2(s_h, s_h) = 0, \tag{5.5}$$

$$(\boldsymbol{u}_h, \varepsilon\nabla_w\varphi + \nabla_w \times \boldsymbol{\psi}) + (\boldsymbol{\psi}_0, \varepsilon\nabla_w s_h) = 0, \qquad \forall \varphi \in M_h, \boldsymbol{\psi} \in \boldsymbol{W}_h, \tag{5.6}$$

$$(\boldsymbol{q}_0, \varepsilon\nabla_w r) + (\boldsymbol{v}, \varepsilon\nabla_w\lambda_h + \nabla_w \times \boldsymbol{q}_h) = 0, \qquad \forall \boldsymbol{v} \in \boldsymbol{V}_h, r \in S_h. \tag{5.7}$$

From (5.5) we have

$$\lambda_0 = \lambda_b, \ \boldsymbol{q}_0 \times \boldsymbol{n} = \boldsymbol{q}_b \times \boldsymbol{n}, \ s_0 = s_b, \quad \text{on } \partial T, \tag{5.8}$$

so that $\lambda_0 \in C(\Omega)$, $s_0 \in C(\Omega)$ and $\boldsymbol{q}_0 \in H_0(curl; \Omega)$. Hence,

$$\nabla\lambda_0 = \nabla_w\lambda_h, \ \nabla \times \boldsymbol{q}_0 = \nabla_w \times \boldsymbol{q}_h. \tag{5.9}$$

Next, by letting $r=0$ and varying $\boldsymbol{v}$ in (5.7) we have

$$\varepsilon\nabla_w\lambda_h+\nabla_w\times\boldsymbol{q}_h=0,$$

which, together with (5.9), implies

$$\varepsilon\nabla\lambda_0+\nabla\times\boldsymbol{q}_0=0. \tag{5.10}$$

From $\boldsymbol{q}_0\in H_0(curl;\Omega)$, we have

$$\begin{aligned}(\varepsilon\nabla\lambda_0+\nabla\times\boldsymbol{q}_0,\nabla\lambda_0)&=(\varepsilon\nabla\lambda_0,\nabla\lambda_0)+(\nabla\times\boldsymbol{q}_0,\nabla\lambda_0)\\&=(\varepsilon\nabla\lambda_0,\nabla\lambda_0)+\langle\boldsymbol{n}\times\boldsymbol{q}_0,\lambda_0\rangle\\&=(\varepsilon\nabla\lambda_0,\nabla\lambda_0).\end{aligned}$$

Thus,

$$(\varepsilon\nabla\lambda_0,\nabla\lambda_0)=0,$$

which gives $\nabla\lambda_0=\boldsymbol{0}$, and hence $\lambda_0\equiv 0$ as a function with mean value 0. This further leads to $\lambda_b\equiv 0$. Thus, from (5.10) we have

$$\nabla\times\boldsymbol{q}_0=0,\qquad \text{in }\Omega.$$

Observe that $\boldsymbol{q}_0$ satisfies

$$(\boldsymbol{q}_0,\varepsilon\nabla_w r)=0\qquad\forall r\in S_h,$$

which leads to $\boldsymbol{q}_0\in H(div_\varepsilon;\Omega)$ and

$$\nabla\cdot(\varepsilon\boldsymbol{q}_0)=0,\quad \langle\boldsymbol{q}_0\cdot\boldsymbol{n}_i,1\rangle_{\Gamma_i}=0,$$

for $i=1,2,\cdots L$. This, together with $\nabla\times\boldsymbol{q}_0=0$ and $\boldsymbol{q}_0\in H_0(curl;\Omega)$ shows that $\boldsymbol{q}_0\equiv 0$, and hence $\boldsymbol{q}_b=\boldsymbol{n}\times(\boldsymbol{q}_b\times\boldsymbol{n})=\boldsymbol{n}\times 0=0$.

Next, from the Helmholtz decomposition (A.1), we have

$$\boldsymbol{u}_h=\varepsilon^{-1}\nabla\times\tilde{\boldsymbol{\psi}}+\nabla\tilde{\phi}+\tilde{\boldsymbol{\eta}},$$

with some $\tilde{\boldsymbol{\eta}}\in\mathbb{H}_{\varepsilon n,0}(\Omega)$ and $\tilde{\boldsymbol{\psi}}\in H_0(curl;\Omega)$ satisfying $\nabla\cdot(\varepsilon\tilde{\boldsymbol{\psi}})=0$ and $\langle\varepsilon\tilde{\boldsymbol{\psi}}\cdot\boldsymbol{n}_i,1\rangle_{\Gamma_i}=0$ for $i=1,\cdots,L$. From $s_2(s_h,s_h)=0$ we have $s_0=s_b$ on ∂T for each element $T\in\mathcal{T}_h$ so that $s_0\in H^1(\Omega)$. It follows that $\nabla_w s_h=\nabla s_0$. If $\mathbb{H}_{\varepsilon n,0}(\Omega)$ has dimension 0, then $\tilde{\boldsymbol{\eta}}=0$. In (5.6), by choosing the test function ϕ and $\boldsymbol{\psi}$ to be the L^2 projection of the corresponding function in the Helmholtz decomposition we arrive at

$$\begin{aligned}0=&(\boldsymbol{u}_h,\varepsilon\nabla_w\mathcal{Q}_h\tilde{\varphi}+\nabla_w\times\mathbb{Q}_h\tilde{\boldsymbol{\psi}})+(\mathbb{Q}_0\tilde{\boldsymbol{\psi}},\varepsilon\nabla_w s_h)\\=&(\boldsymbol{u}_h,\mathcal{Q}_h\varepsilon\nabla\tilde{\varphi}+\mathcal{Q}_h\nabla\times\tilde{\boldsymbol{\psi}})+(\tilde{\boldsymbol{\psi}},\varepsilon\nabla s_0)\\=&(\boldsymbol{u}_h,\varepsilon\nabla\tilde{\varphi}+\nabla\times\tilde{\boldsymbol{\psi}})+(\tilde{\boldsymbol{\psi}},\varepsilon\nabla s_0)\\=&(\varepsilon\boldsymbol{u}_h,\boldsymbol{u}_h-\tilde{\boldsymbol{\eta}})+(\tilde{\boldsymbol{\psi}},\varepsilon\nabla s_0)\\=&(\varepsilon(\boldsymbol{u}_h-\tilde{\boldsymbol{\eta}}),\boldsymbol{u}_h-\tilde{\boldsymbol{\eta}}),\end{aligned} \tag{5.11}$$

which leads to $\boldsymbol{u}_h-\tilde{\boldsymbol{\eta}}=0$; i.e., $\boldsymbol{u}_h$ is a harmonic function. As a harmonic function and piecewise polynomial of degree k, the first term on the left-hand side of (5.6) becomes to be zero for all test functions $\varphi\in M_h$ and $\boldsymbol{\psi}\in\boldsymbol{W}_h$. It follows that $\nabla_w s_h=0$ so that $\nabla s_0=\nabla_w s_h=0$ and hence $s_0\equiv 0$, so is $s_b\equiv 0$. □

The following is our main result concerning the solution existence and uniqueness of the numerical scheme (4.2).

Theorem 5.3. *The PDWG finite element scheme (4.2) has one and only one solution for all the components except $\boldsymbol{u}_h$. The solution $\boldsymbol{u}_h$ is unique up to a harmonic function $\boldsymbol{\eta}_h\in\mathbb{H}_{\varepsilon n,0}(\Omega)$ that is a piecewise polynomial of degree k.*

Remark 5.4. For the PDWG element of lowest order (i.e., $k=0$), any $\boldsymbol{\eta}_h$ in the kernel K_h of the PDWG operator of (4.2) would be a piecewise constant vector field that is continuous across each interior element interface and has vanishing value on the domain boundary along the normal direction. It follows that $\boldsymbol{\eta}_h\equiv 0$, or equivalently, the PDWG finite element scheme (4.2) has one and only one solution for all the components.

6. Error analysis

For the exact solution $\{\boldsymbol{u};s=0\}$ of the div-curl system, we have from (3.1) and (3.2) that

$$\begin{aligned}B_h(\mathcal{Q}_h\boldsymbol{u},\mathcal{Q}_h s;\varphi,\boldsymbol{\psi})=&(\mathcal{Q}_h\boldsymbol{u},\varepsilon\nabla_w\varphi+\nabla_w\times\boldsymbol{\psi})+(\boldsymbol{\psi}_0,\varepsilon\nabla_w\mathcal{Q}_h s)\\=&(\mathcal{Q}_h\boldsymbol{u},\varepsilon\nabla\varphi_0+\nabla\times\boldsymbol{\psi}_0)\\&+\langle\mathcal{Q}_h\boldsymbol{u},\varepsilon\boldsymbol{n}(\varphi_b-\varphi_0)+(\boldsymbol{\psi}_0-\boldsymbol{\psi}_b)\times\boldsymbol{n}\rangle_{\mathcal{E}_h}\\=&(\boldsymbol{u},\varepsilon\nabla\varphi_0+\nabla\times\boldsymbol{\psi}_0)\\&+\langle\mathcal{Q}_h\boldsymbol{u},\varepsilon\boldsymbol{n}(\varphi_b-\varphi_0)+(\boldsymbol{\psi}_0-\boldsymbol{\psi}_b)\times\boldsymbol{n}\rangle_{\mathcal{E}_h}\\=&-(\nabla\cdot(\varepsilon\boldsymbol{u}),\varphi_0)+(\nabla\times\boldsymbol{u},\boldsymbol{\psi}_0)\\&+\langle\boldsymbol{u},\varepsilon\boldsymbol{n}(\varphi_0-\varphi_b)+(\boldsymbol{\psi}_b-\boldsymbol{\psi}_0)\times\boldsymbol{n}\rangle_{\mathcal{E}_h}\\&+\langle\mathcal{Q}_h\boldsymbol{u},\varepsilon\boldsymbol{n}(\varphi_b-\varphi_0)+(\boldsymbol{\psi}_0-\boldsymbol{\psi}_b)\times\boldsymbol{n}\rangle_{\mathcal{E}_h}\\&+\langle\phi_1,\varphi_b\rangle_{\partial\Omega}\\=&\langle\phi_1,\varphi_b\rangle_{\partial\Omega}-(f,\varphi_0)+(\boldsymbol{g},\boldsymbol{\psi}_0)\\&+\langle\boldsymbol{u}-\mathcal{Q}_h\boldsymbol{u},\varepsilon\boldsymbol{n}(\varphi_0-\varphi_b)+(\boldsymbol{\psi}_b-\boldsymbol{\psi}_0)\times\boldsymbol{n}\rangle_{\mathcal{E}_h}.\end{aligned} \tag{6.1}$$

Combining the above equation with the fact that $\lambda=0$, $\boldsymbol{q}=0$ we obtain

$$\begin{aligned}&s_1(\mathcal{Q}_h\lambda-\lambda_h,\mathbb{Q}_h\boldsymbol{q}-\boldsymbol{q}_h;\varphi,\boldsymbol{\psi})+B(\mathcal{Q}_h\boldsymbol{u}-\boldsymbol{u}_h,\mathcal{Q}_h s-s_h;\varphi,\boldsymbol{\psi})\\=&\langle\boldsymbol{u}-\mathcal{Q}_h\boldsymbol{u},\varepsilon\boldsymbol{n}(\varphi_0-\varphi_b)+(\boldsymbol{\psi}_b-\boldsymbol{\psi}_0)\times\boldsymbol{n}\rangle_{\mathcal{E}_h}.\end{aligned} \tag{6.2}$$

The second error equation can be easily obtained as follows:

$$-s_2(\mathcal{Q}_h s-s_h,r)+B(\boldsymbol{v},r;\mathcal{Q}_h\lambda-\lambda_h,\mathbb{Q}_h\boldsymbol{q}-\boldsymbol{q}_h)=0, \tag{6.3}$$

where we have used the fact that $s=0$, $\boldsymbol{q}=0$, and $\lambda=0$.

Denote the error functions by

$$e_{\boldsymbol{u}}=\mathcal{Q}_h\boldsymbol{u}-\boldsymbol{u}_h,\ e_s=\mathcal{Q}_h s-s_h,\ e_\lambda=\mathcal{Q}_h\lambda-\lambda_h,\ e_{\boldsymbol{q}}=\mathbb{Q}_h\boldsymbol{q}-\boldsymbol{q}_h.$$

Theorem 6.1. *For the numerical solution $\boldsymbol{u}_h$, s_h, λ_h, $\boldsymbol{q}_h$ arising from the PDWG scheme (4.2), the following estimate holds true:*

$$|||(e_\lambda,e_{\boldsymbol{q}})|||+|||e_s|||\lesssim h^{k+\theta}\|\boldsymbol{u}\|_{k+\theta}, \tag{6.4}$$

provided that $\boldsymbol{u}\in[H^{k+\theta}(\Omega)]^3$ for $\theta\in(1/2,1]$.

Proof. From (6.2) and (6.3) we have

$$s_1(e_\lambda,e_{\boldsymbol{q}};e_\lambda,e_{\boldsymbol{q}})+s_2(e_s,e_s)=\langle\boldsymbol{u}-\mathcal{Q}_h\boldsymbol{u},\varepsilon\boldsymbol{n}(e_{\lambda,0}-e_{\lambda,b})+(e_{\boldsymbol{q},b}-e_{\boldsymbol{q},0})\times\boldsymbol{n}\rangle_{\mathcal{E}\mathcal{E}_h},$$

which leads to

$$|||(e_\lambda,e_{\boldsymbol{q}})|||^2+|||e_s|||^2\lesssim h^{k+\theta}\|\boldsymbol{u}\|_{k+\theta}|||(e_\lambda,e_{\boldsymbol{q}})|||, \tag{6.5}$$

where $\theta\in(1/2,1]$ and k is the order of polynomials for the finite element space $\boldsymbol{V}_h$. This completes the proof of the theorem. □

To derive an estimate for the error function $e_{\boldsymbol{u}}$, we use the Helmholtz decomposition (A.1) to obtain a $\tilde{\phi}\in H^1(\Omega)$, $\tilde{\boldsymbol{\psi}}\in H_0(curl;\Omega)$, and $\tilde{\boldsymbol{\eta}}\in\mathbb{H}_{\varepsilon n,0}(\Omega)$ such that

$$e_{\boldsymbol{u}}=\varepsilon^{-1}\nabla\times\tilde{\boldsymbol{\psi}}+\nabla\tilde{\phi}+\tilde{\boldsymbol{\eta}}. \tag{6.6}$$

Assume the following H^α-regularity holds true for some fixed $\alpha\in(1/2,1]$:

$$\|\tilde{\boldsymbol{\psi}}\|_\alpha+\|\tilde{\phi}\|_\alpha\lesssim\|e_{\boldsymbol{u}}-\tilde{\boldsymbol{\eta}}\|_0. \tag{6.7}$$

The following is the main convergence result of this paper.

Theorem 6.2. *Let $\boldsymbol{u}$ be a solution of the div-curl system (1.1)-(1.3). Assume that the Helmholtz decomposition (6.6) has the H^{α}-regularity estimate (6.7). For a numerical solution $\boldsymbol{u}_h$, s_h, λ_h, $\boldsymbol{q}_h$ arising from (4.2), there exists a harmonic function $\tilde{\boldsymbol{\eta}} \in \mathbb{H}_{\varepsilon n,0}(\Omega)$ such that the following estimate holds true:*

$$\|\varepsilon^{1/2}(\boldsymbol{u}_h + \tilde{\boldsymbol{\eta}} - Q_h\boldsymbol{u})\| \lesssim h^{k+\theta+\alpha-1}\|\boldsymbol{u}\|_{k+\theta}, \tag{6.8}$$

provided that $\boldsymbol{u} \in [H^{k+\theta}(\Omega)]^3$ for $\theta \in (1/2, 1]$.

Proof. From the first error equation (6.2), we have

$$s_1(e_\lambda, e_{\boldsymbol{q}}; \varphi, \boldsymbol{\psi}) + B(e_{\boldsymbol{u}}, e_s; \varphi, \boldsymbol{\psi}) = \langle \boldsymbol{u} - Q_h\boldsymbol{u}, \varepsilon\boldsymbol{n}(\varphi_0 - \varphi_b) + (\boldsymbol{\psi}_b - \boldsymbol{\psi}_0)\times\boldsymbol{n}\rangle_{\mathcal{E}_h}. \tag{6.9}$$

Recall the Helmholtz decomposition (6.6) for the error function $e_{\boldsymbol{u}}$. By letting $\varphi = Q_h\tilde{\phi}$ and $\boldsymbol{\psi} = Q_h\tilde{\boldsymbol{\psi}}$, we obtain from Lemma 5.1

$$\begin{aligned} B(e_{\boldsymbol{u}}, e_s; \varphi, \boldsymbol{\psi}) &= (e_{\boldsymbol{u}}, \varepsilon\nabla_w Q_h\tilde{\phi} + \nabla_w\times\mathbb{Q}_h\tilde{\boldsymbol{\psi}}) + (\mathbb{Q}_0\tilde{\boldsymbol{\psi}}, \varepsilon\nabla_w e_s) \\ &= (e_{\boldsymbol{u}}, \varepsilon Q_h\nabla_w\tilde{\phi} + Q_h\nabla_w\times\tilde{\boldsymbol{\psi}}) + (\mathbb{Q}_0\tilde{\boldsymbol{\psi}}, \varepsilon\nabla_w e_s) \\ &= (e_{\boldsymbol{u}}, \varepsilon\nabla\tilde{\phi} + \nabla\times\tilde{\boldsymbol{\psi}}) + (\mathbb{Q}_0\tilde{\boldsymbol{\psi}}, \varepsilon\nabla_w e_s) \\ &= (\varepsilon e_{\boldsymbol{u}}, e_{\boldsymbol{u}} - \tilde{\boldsymbol{\eta}}) + (\varepsilon\mathbb{Q}_0\tilde{\boldsymbol{\psi}}, \nabla_w e_s) \\ &= (\varepsilon(e_{\boldsymbol{u}} - \tilde{\boldsymbol{\eta}}), e_{\boldsymbol{u}} - \tilde{\boldsymbol{\eta}}) + (\varepsilon\mathbb{Q}_0\tilde{\boldsymbol{\psi}}, \nabla_w e_s). \end{aligned} \tag{6.10}$$

From the definition of the weak gradient we have

$$\begin{aligned} (\varepsilon\mathbb{Q}_0\tilde{\boldsymbol{\psi}}, \nabla_w e_s) &= (\varepsilon\mathbb{Q}_0\tilde{\boldsymbol{\psi}}, \nabla e_{s,0}) + \langle \varepsilon\mathbb{Q}_0\tilde{\boldsymbol{\psi}}\cdot\boldsymbol{n}, e_{s,b} - e_{s,0}\rangle_{\mathcal{E}_h} \\ &= (\varepsilon\tilde{\boldsymbol{\psi}}, \nabla e_{s,0}) + \langle \varepsilon\mathbb{Q}_0\tilde{\boldsymbol{\psi}}\cdot\boldsymbol{n}, e_{s,b} - e_{s,0}\rangle_{\mathcal{E}_h} \\ &= -(\nabla\cdot(\varepsilon\tilde{\boldsymbol{\psi}}), \nabla e_{s,0}) + \langle \varepsilon\tilde{\boldsymbol{\psi}}\cdot\boldsymbol{n}, e_{s,0}\rangle_{\mathcal{E}_h} \\ &\quad + \langle \varepsilon\mathbb{Q}_0\tilde{\boldsymbol{\psi}}\cdot\boldsymbol{n}, e_{s,b} - e_{s,0}\rangle_{\mathcal{E}_h} \\ &= \langle \varepsilon\tilde{\boldsymbol{\psi}}\cdot\boldsymbol{n}, e_{s,0} - e_{s,b}\rangle_{\mathcal{E}_h} + \langle \varepsilon\mathbb{Q}_0\tilde{\boldsymbol{\psi}}\cdot\boldsymbol{n}, e_{s,b} - e_{s,0}\rangle_{\mathcal{E}_h} \\ &= \langle \varepsilon(\tilde{\boldsymbol{\psi}} - \mathbb{Q}_0\tilde{\boldsymbol{\psi}})\cdot\boldsymbol{n}, e_{s,0} - e_{s,b}\rangle_{\mathcal{E}_h}. \end{aligned}$$

Substituting the above into (6.10) then (6.9) yields

$$\begin{aligned} \|\varepsilon^{1/2}(e_{\boldsymbol{u}} - \tilde{\boldsymbol{\eta}})\|^2 &= B(e_{\boldsymbol{u}}, e_s; \varphi, \boldsymbol{\psi}) - \langle \varepsilon(\tilde{\boldsymbol{\psi}} - \mathbb{Q}_0\tilde{\boldsymbol{\psi}})\cdot\boldsymbol{n}, e_{s,0} - e_{s,b}\rangle_{\mathcal{E}_h} \\ &= \langle \boldsymbol{u} - Q_h\boldsymbol{u}, \varepsilon\boldsymbol{n}(\varphi_0 - \varphi_b) + (\boldsymbol{\psi}_b - \boldsymbol{\psi}_0)\times\boldsymbol{n}\rangle_{\mathcal{E}_h} \\ &\quad - s_1(e_\lambda, e_{\boldsymbol{q}}; \varphi, \boldsymbol{\psi}) - \langle \varepsilon(\tilde{\boldsymbol{\psi}} - \mathbb{Q}_0\tilde{\boldsymbol{\psi}})\cdot\boldsymbol{n}, e_{s,0} - e_{s,b}\rangle_{\mathcal{E}_h}, \end{aligned}$$

which leads to

$$\begin{aligned} \|\varepsilon^{1/2}(e_{\boldsymbol{u}} - \tilde{\boldsymbol{\eta}})\|^2 &\lesssim h^{\theta}\|\boldsymbol{u} - Q_h\boldsymbol{u}\|_{\theta}|||(\varphi, \boldsymbol{\psi})||| + |||(e_\lambda, e_{\boldsymbol{q}})|||||(\varphi, \boldsymbol{\psi})||| \\ &\quad + h^{\alpha+(\gamma-1)/2}\|\tilde{\boldsymbol{\psi}}\|_{\alpha}|||e_s|||. \end{aligned}$$

It can be proved that

$$|||(\varphi, \boldsymbol{\psi})||| \lesssim h^{\alpha-1}\|(\tilde{\varphi}, \tilde{\boldsymbol{\psi}})\|_{\alpha}.$$

It follows that

$$\begin{aligned} \|\varepsilon^{1/2}(e_{\boldsymbol{u}} - \tilde{\boldsymbol{\eta}})\|^2 &\lesssim h^{\theta}\|\boldsymbol{u} - Q_h\boldsymbol{u}\|_{\theta}h^{\alpha-1}\|(\tilde{\varphi}, \tilde{\boldsymbol{\psi}})\|_{\alpha} + |||(e_\lambda, e_{\boldsymbol{q}})|||h^{\alpha-1}\|(\tilde{\varphi}, \tilde{\boldsymbol{\psi}})\|_{\alpha} \\ &\quad + h^{\alpha+(\gamma-1)/2}\|\tilde{\boldsymbol{\psi}}\|_{\alpha}|||e_s|||, \end{aligned}$$

so that

$$\begin{aligned} \|\varepsilon^{1/2}(e_{\boldsymbol{u}} - \tilde{\boldsymbol{\eta}})\| &\lesssim h^{\alpha+\theta-1}\|\boldsymbol{u} - Q_h\boldsymbol{u}\|_{\theta} + h^{\alpha-1}|||(e_\lambda, e_{\boldsymbol{q}})||| + h^{\alpha+(\gamma-1)/2}|||e_s||| \\ &\lesssim h^{k+\theta+\alpha-1}\|\boldsymbol{u}\|_{k+\theta}, \end{aligned}$$

which gives rise to the error estimate (6.8). □

7. Numerical experiments

In this section, we present some numerical results for the PDWG finite element method proposed and analyzed in previous sections. For simplicity, we choose the lowest order PDWG element; i.e., $k = 0$ so that the solution $\boldsymbol{u}$ is approximated by discontinuous piecewise constant vector fields. The exact solution $\boldsymbol{u}$ has various regularities ranging from smooth to corner singular. The computational domain includes convex and non-convex polyhedral regions; some have cavities or multiple toroidal topology. The implementation uses an open-source and publicly available MATLAB package iFEM [6]. The computational domain is first partitioned into cubes, and each cube is further divided into 6 tetrahedra of equi-volume to form a shape-regular finite element partition. On each tetrahedral element T with boundary $\partial T = \cup_{i=1}^4 F_i$, the local finite element space consists of functions given as follows: for $k = 0, 1$

$$\boldsymbol{u}_h|_T \in \left[P_k(T)\right]^3, \tag{7.1}$$

$$s_h|_T = \left\{s_0, s_b\right\} \in \left\{P_k(T), \Pi_{i=1}^4 P_k(F_i)\right\}, \tag{7.2}$$

$$\varphi_h|_T = \left\{\varphi_0, \varphi_b\right\} \in \left\{P_k(T), \Pi_{i=1}^4 P_k(F_i)\right\}, \tag{7.3}$$

$$\boldsymbol{\psi}_h|_T = \left\{\boldsymbol{\psi}_0, \boldsymbol{\psi}_b\right\} \in \left\{\left[P_k(T)\right]^3, T_k(\partial T)\right\}. \tag{7.4}$$

When the true solution is singular, we choose $k = 0$, and $T_0(\partial T)$ is tangential to the boundary and is given by

$$T_0(\partial T) := \{\boldsymbol{\psi} : \boldsymbol{\psi}_{F_{i,j}} \in \left[P_0(F_i)\right]^3 \times \boldsymbol{n}_{F_i},\ j = 1, 2 \text{ and } i = 1, 2, 3, 4\},$$

where $\boldsymbol{n}_{F_i}$ is the outer unit normal vector to face F_i. The basis functions for the first three spaces are straightforward. For $T_0(\partial T)$, on each face F_i we choose the normalized vectors representing the directional vector of any 2 edges ($j = 1, 2$) among 3 on ∂F_i, such that its weak curl is the co-normal vector of this edge with respect to F_i ($i = 1, 2, 3, 4$),

$$\nabla_w \times \left\{\boldsymbol{0}, \boldsymbol{\psi}_{F_{i,j}}\right\} = 3\boldsymbol{\psi}_{F_{i,j}} \times (\nabla\zeta_i),$$

where ζ_i is the barycentric coordinate associated with the vertex opposite to face F_i.

When the true solution has extra smoothness than being H^1-regular, we compare $k = 0$ and $k = 1$ cases. We choose the linear Nédélec elements and their facewise tangential projections locally as the basis functions for $P^1(T)$ and $P^1(F_i)$, respectively.

For each test problem, we specify a vector field $\boldsymbol{u}$ as the true solution, while the right-hand sides of the div-curl system (1.1)-(1.3) are computed accordingly. We shall evaluate the following errors for the PDWG finite element solution:

$$\|\varepsilon^{1/2}\mathbf{e}_{\boldsymbol{u}}\| := \|\varepsilon^{1/2}(\boldsymbol{u} - \boldsymbol{u}_h)\|, \tag{7.5}$$

$$|||(e_\lambda, \mathbf{e}_{\boldsymbol{q}})||| := \left(s_1(\lambda_h, \boldsymbol{q}_h; \lambda_h, \boldsymbol{q}_h)\right)^{1/2}, \tag{7.6}$$

$$|||e_s||| := \left(s_2(s_h; s_h)\right)^{1/2}, \tag{7.7}$$

where the $L^2(\Omega)$-norm $\|\varepsilon^{1/2}\mathbf{e}_{\boldsymbol{u}}\|$ is computed by using a higher order Gaussian quadrature on each element.

7.1. Example 1

$\Omega = (0, 1)^3$, $\varepsilon = \mathrm{diag}(3, 2, 1)$, the true solution $\boldsymbol{u} \in \left(H^1(\Omega)\right)^3$ is given by

$$\boldsymbol{u}(x, y, z) = \begin{pmatrix} \sin(\pi x)\cos(\pi y) \\ -\sin(\pi y)\cos(\pi x) \\ 0 \end{pmatrix} + \begin{pmatrix} x \\ y \\ z \end{pmatrix}.$$

The performance of the PDWG finite element solution for this test problem is illustrated in Table 1. It can be seen that $\mathbf{e}_{\boldsymbol{u}}$, $(e_\lambda, \mathbf{e}_{\boldsymbol{q}})$, and e_s all have optimal rate of convergence for $k = 0$ as shown in Theorem 6.2. The plot of the true solution and the PDWG approximation can be found in Fig. 1.

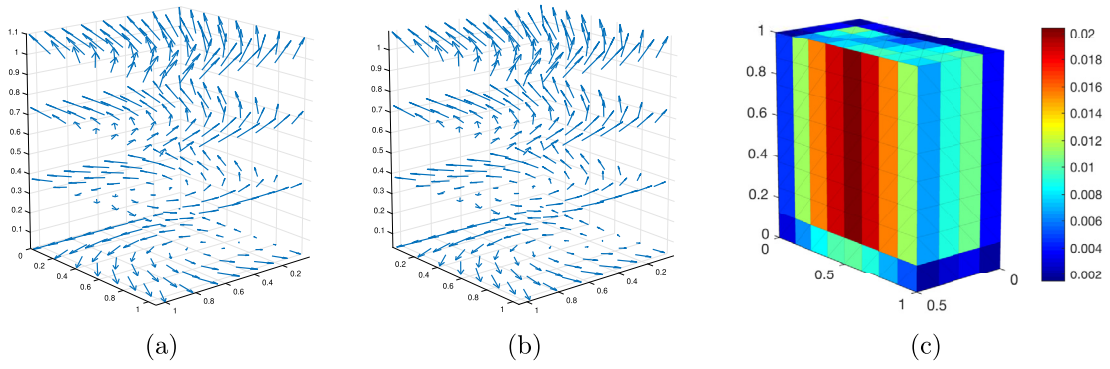

Fig. 1. The true solution vector field shown in (a) of Example 1 versus the WG approximation (b). The vector fields are plotted on four $z = c$ planes. The distribution of $\|\varepsilon^{1/2}\mathbf{e}_{\boldsymbol{u}}\|_T$ locally is plotted in (c) on the cut plane $x = 1/2$ with $h = 1/8$.

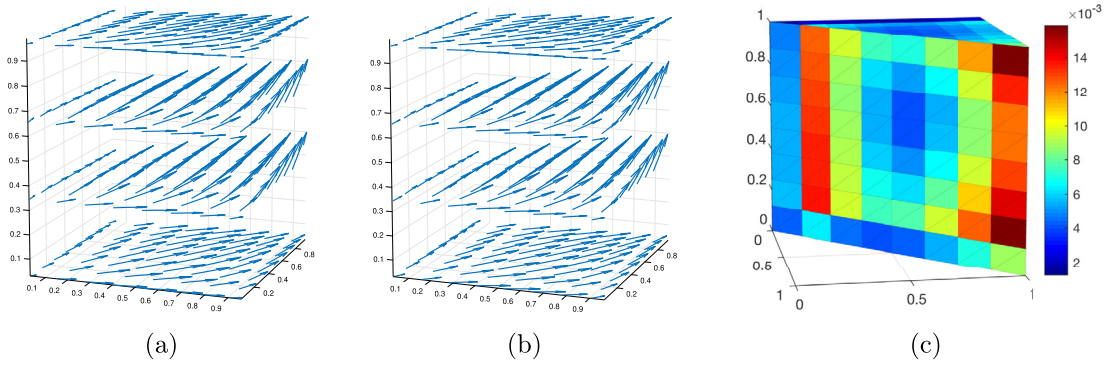

Fig. 2. The true solution vector field shown in (a) of Example 2 versus the PDWG approximation (b). The vector fields are plotted on four $z = c$ planes. The distribution of $\|\varepsilon^{1/2}\mathbf{e}_{\boldsymbol{u}}\|_T$ locally is plotted in (c) on the cut plane $x = y$ with $h = 1/8$.

Table 1
Errors and corresponding rates of convergence for Example 1.

$1/h$	$\|\varepsilon^{1/2}\mathbf{e}_{\boldsymbol{u}}\|$	Rate	$\|\|\|(e_\lambda, \mathbf{e}_{\boldsymbol{q}})\|\|\|$	Rate	$\|\|\|e_s\|\|\|$	Rate
2	1.64e-1	–	2.95e-1	–	3.96e-2	–
4	8.16e-2	1.01	1.68e-1	0.82	1.86e-2	1.09
8	3.93e-2	1.03	8.72e-2	0.88	8.79e-3	1.09
16	1.93e-2	1.03	4.41e-2	0.98	4.48e-3	0.98

Table 2
Errors and corresponding rates of convergence for Example 2 with $k = 0$ in (4.2).

$1/h$	$\|\varepsilon^{1/2}\mathbf{e}_{\boldsymbol{u}}\|$	Rate	$\|\|\|(e_\lambda, \mathbf{e}_{\boldsymbol{q}})\|\|\|$	Rate	$\|\|\|e_s\|\|\|$	Rate
2	1.13e-1	–	2.07e-1	–	1.74e-2	–
4	5.20e-2	1.12	1.20e-1	0.78	1.05e-2	0.73
8	2.50e-2	1.05	6.27e-2	0.94	5.53e-3	0.93
16	1.23e-2	1.02	3.18e-2	0.98	2.82e-3	0.97

7.2. Example 2

The second example is adopted from [16] with $\varepsilon = I$ and a singular solution in $\left(H^{1+\frac{2}{3}-\epsilon}(\Omega)\right)^3$ with $\Omega = (0,1)^3$:

$$\boldsymbol{u}(x,y,z) = \begin{pmatrix} x(1-x) \\ y(1-y) \\ r^{2/3}\sin(2\theta)z(1-z) \end{pmatrix},$$

in which $r = \sqrt{x^2+y^2}$, and $\theta = \arctan(y/x) + c$ in the cylindrical coordinates. Similar to Example 1, for $k = 0$, the result in Table 2 shows optimal rates of convergence for $\mathbf{e}_{\boldsymbol{u}}$, while slightly sub-optimal in the coarsest two levels for $(e_\lambda, \mathbf{e}_{\boldsymbol{q}})$, and e_s, respectively. When $k = 1$, i.e., the local finite element approximation spaces are all linear, the result in Table 3 shows sub-optimal rates for $\mathbf{e}_{\boldsymbol{u}}$ and $(e_\lambda, \mathbf{e}_{\boldsymbol{q}})$ in the coarsest two levels, and then optimal once the mesh gets finer thus leveraging the extra smoothness of $\boldsymbol{u}$. The plot of the true solution and the PDWG approximation for $k = 0$ can be found in Fig. 2.

Table 3
Errors and corresponding rates of convergence for Example 2 with $k = 1$ in (4.2).

$1/h$	$\|\varepsilon^{1/2}\mathbf{e}_{\boldsymbol{u}}\|$	Rate	$\|\|\|(e_\lambda, \mathbf{e}_{\boldsymbol{q}})\|\|\|$	Rate	$\|\|\|e_s\|\|\|$	Rate
2	1.38e-2	–	7.69e-2	–	5.39e-3	–
4	4.89e-3	1.50	2.50e-2	1.62	1.51e-3	1.84
8	1.46e-3	1.62	7.64e-3	1.67	4.52e-4	1.79
16	4.25e-4	1.76	2.44e-3	1.68	1.45e-4	1.69

7.3. Example 3

This test problem is defined on a non-convex domain $\Omega = (-1,1)^2 \times (0,1)\backslash[0,1] \times [-1,0] \times [0,1]$ with $\varepsilon = I$ and the singular solution in $\left(H^{2/3-\epsilon}(\Omega)\right)^3$:

$$\boldsymbol{u} = \nabla \times \left\langle 0, 0, r^{2/3}\sin\left(\frac{2}{3}\theta\right)\right\rangle.$$

The true solution $\boldsymbol{u}$ is a solenoidal vector field (see Fig. 3). Similar to Example 2, $r = \sqrt{x^2+y^2}$ and $\theta = \arctan(y/x) + c$ are the cylindrical coordinates, where c is chosen such that $\boldsymbol{u} \in H(div) \cap H(curl)$. Since $\boldsymbol{u}(x,y,z)$ has unbounded derivatives as (x,y,z) approaches $\{x = 0, y = 0\} \cap \partial\Omega$, the Gaussian quadrature would yield large error on elements with boundary intersecting z-axis. To overcome this difficulty, we replace the true solution by its L^2-projection in the error computation:

$$\|\varepsilon^{1/2}\mathbf{e}_{Q_h\boldsymbol{u}}\| := \|\varepsilon^{1/2}(Q_h\boldsymbol{u} - \boldsymbol{u}_h)\|.$$

It is observed that $\mathbf{e}_{Q_h\boldsymbol{u}}$, $(e_\lambda, \mathbf{e}_{\boldsymbol{q}})$, and e_s all have maximum possible rate of convergence ($\approx h^{2/3}$) on the finer meshes (see Table 4). The plot of the true solution and the PDWG approximation can be found in Fig. 4.

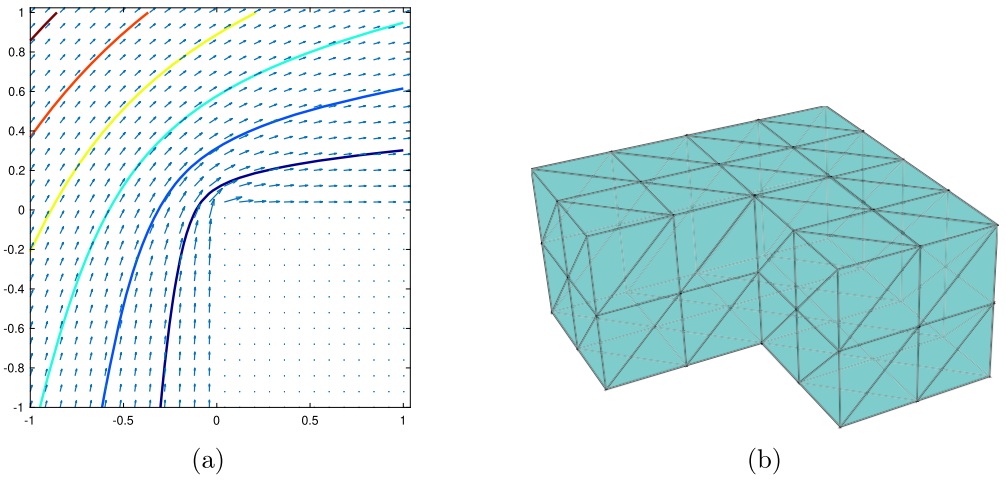

Fig. 3. The true solution vector field shown in (a) of Example 3 view from above on $z = 1/4$ plane together with the level set of its z-component. A coarse mesh ($h = 1/2$) used in Example 3 is illustrated in (b).

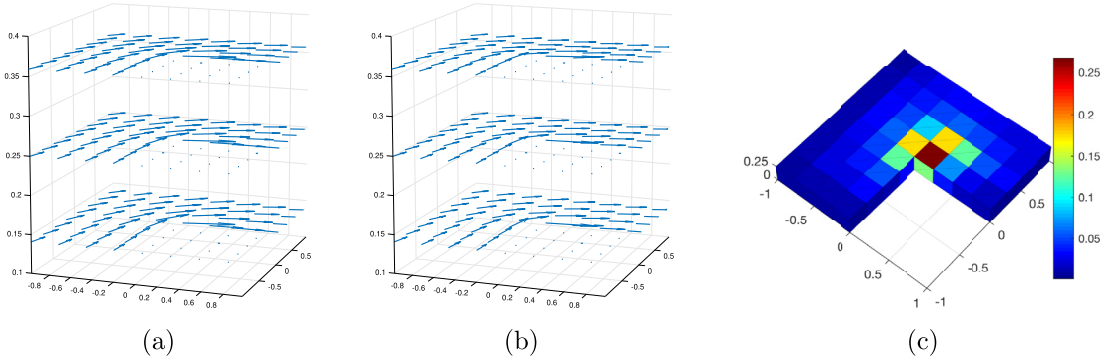

Fig. 4. The vector field of $Q_h\boldsymbol{u}$ is shown in (a) of Example 3 versus the PDWG approximation (b). The vector fields are plotted on several $z = c$ planes. The distribution of $\|\epsilon^{1/2}\mathbf{e}_{Q_h\boldsymbol{u}}\|_T$ locally is plotted in (c) on the cut plane $z = 1/4$ when $h = 1/8$.

Table 4
Errors and corresponding rates of convergence for Example 3.

$1/h$	$\|\|\|\epsilon^{1/2}\mathbf{e}_{Q_h\boldsymbol{u}}\|\|\|$	Rate	$\|\|\|(e_\lambda, \mathbf{e}_q)\|\|\|$	Rate	$\|\|\|e_s\|\|\|$	Rate
2	5.29e-2	–	3.35e-1	–	4.99e-2	–
4	3.13e-2	0.75	2.19e-1	0.61	3.30e-2	0.60
8	1.91e-2	0.72	1.41e-1	0.63	2.14e-2	0.62
16	1.16e-2	0.72	9.03e-2	0.65	1.37e-2	0.64

Table 5
Errors and corresponding rates of convergence for Example 4.

$1/h$	$\|\|\|\epsilon^{1/2}\mathbf{e}_{Q_h\boldsymbol{u}}\|\|\|$	Rate	$\|\|\|(e_\lambda, \mathbf{e}_q)\|\|\|$	Rate	$\|\|\|e_s\|\|\|$	Rate
2	1.90-1	–	2.51e-1	–	2.04e-2	–
4	1.23e-1	0.63	1.93e-1	0.38	1.69e-2	0.27
8	7.78e-2	0.66	1.35e-1	0.51	1.24e-2	0.44
16	4.91e-2	0.66	9.03e-2	0.58	8.47e-3	0.55

7.4. Example 4

This test problem is defined on the domain $\Omega = (-3/2, 1/2)^3 \backslash [-1, 0]^3$ such that the domain boundary $\partial\Omega$ consists of two disjoint connected components $\Gamma_0 = \partial(-3/2, 1/2)^3$ and $\Gamma_1 = \partial(-1, 0)^3$. The true solution is given by

$$\boldsymbol{u} = \nabla(r^{1/6}), \quad \text{with} \quad r = \sqrt{x^2 + y^2 + z^2}.$$

It is straightforward to see that $\boldsymbol{u}$ is singular near $(0, 0, 0)$ which is one of the nonconvex corners of the cavity (see Fig. 5), and $\boldsymbol{u} \in [H^{2/3-\epsilon}(\Omega)]^3$.

Table 5 illustrates the convergence of the PDWG method for Example 4. It can be seen that $\mathbf{e}_{Q_h\boldsymbol{u}}$ has the optimal rate of convergence of $O(h^{2/3})$. On the other hand, the convergence for $(e_\lambda, \mathbf{e}_q)$ and e_s seems to be approximating the optimal rate in this numerical test.

For $s = \{s_0, s_b\}$, when solving the algebraic system, we seek a constant c_1 such that $s_b|_{\Gamma_1} = c_1$ through a simple post-processing by treating $s_b|_{\Gamma_1}$ as the fixed DoFs first. Denote by $\mathbf{U}$ the vector representation of the solution $(\boldsymbol{u}_h, \lambda_h, s_h, \boldsymbol{q}_h)$, and $\mathbf{U}_s = c_1\mathbf{S}$, $\mathbf{S} = (0, \cdots, 1, \cdots, 1, \cdots, 0)$, the indicator vector representing a solution with $s_b = 1$ on Γ_1 while all other DoFs are zero. Let A be the full stiffness matrix including from all nodal bases (including boundary faces), while A^{int} be the stiffness matrix for all the free DoFs: including the interior DoFs for $\boldsymbol{u}_h$, s_h, and $\boldsymbol{q}_h$, all except 1 fixed DoF for λ_h. Let R be the restriction operator such that $R : \mathbf{U} \mapsto \mathbf{U}^{\text{int}}$, which is the vector representing all the aforementioned free DoFs. First we solve the following algebraic system:

$$A^{\text{int}}\mathbf{U}^{\text{int}} = R\mathbf{F},$$

where $\mathbf{F}$ is the full vector of the right hand side. Then the constant c_1 is sought by solving the following minimization problem:

$$c_1 = \underset{a\in\mathbb{R}}{\text{argmin}} \|A(\mathbf{U}^{\text{int}} + a\mathbf{S}) - F\|_{\ell^2}.$$

The plot of the projection of the true solution and the PDWG approximation is shown in Fig. 6.

7.5. Example 5

In this example we consider singular solutions in the following vector potential form on a toroidal domain: $\Omega = \left((-1, \frac{1}{2})^2 \backslash [-\frac{1}{2}, 0]^2\right) \times (0, \frac{1}{2})$

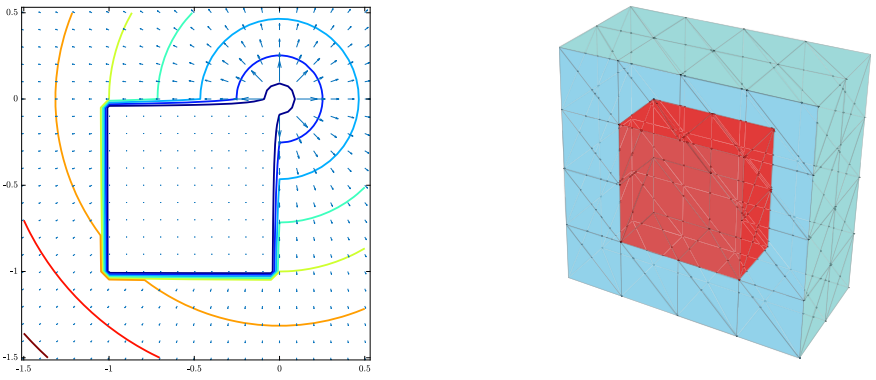

Fig. 5. (a): plot of the true solution field of Example 4, view from above on $z=0$ plane. (b): a coarse mesh ($h=1/2$) used in Example 4 cut by the plane $x=0$, with boundary faces of Γ_1 being highlighted in red.

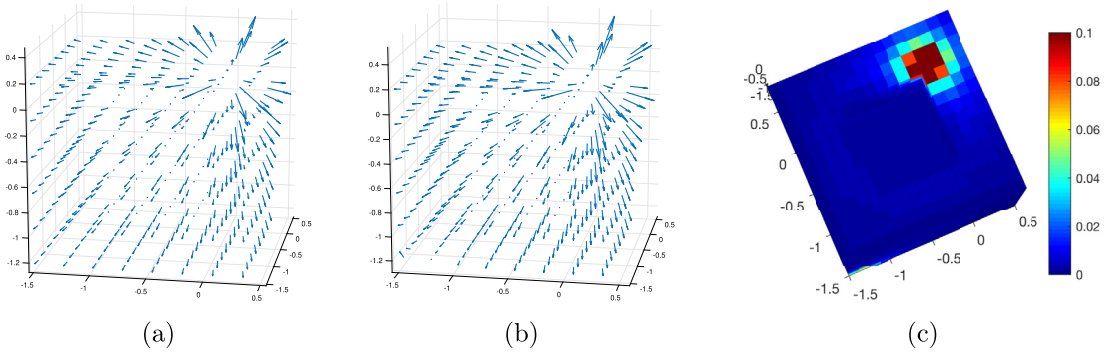

Fig. 6. The vector field $\mathcal{Q}_h\boldsymbol{u}$ is shown in (a) for Example 4 versus the PDWG approximation (b). The vector fields are plotted on several $z=c$ planes. The error distribution of $\|\varepsilon^{1/2}\mathbf{e}_{\mathcal{Q}_h\boldsymbol{u}}\|_T$ is plotted in (c) on the cut plane $z=0$ with meshsize $h=1/8$.

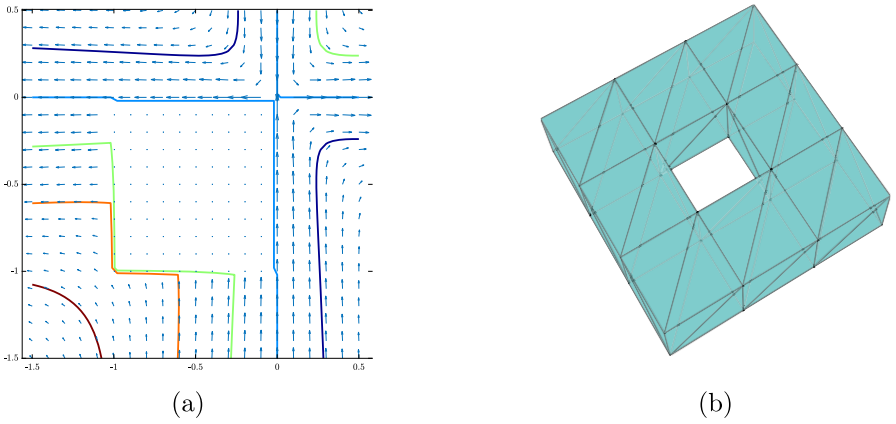

Fig. 7. Example 5: Plot of the singular true solution vector field with $\gamma=3/4$ and $\alpha=2$ is shown in (a), view from above on $z=0$ plane. The level set contours are for the z-component of the vector potential. The coarse mesh ($h=1/2$) is shown in (b).

$$\boldsymbol{u}=\nabla\times\left\langle 0,0,r^{\gamma}\sin\left(\alpha\theta\right)\right\rangle,$$

where r and θ are the cylindrical coordinates defined as in Example 3. It can be verified that for $\gamma\neq 1$, $\boldsymbol{u}\in\left(H^{\gamma-\epsilon}(\Omega)\right)^3$, and for $\gamma<1$, this vector field is singular near a non-convex corner centered at z-axis (see Fig. 7).

Unlike Example 7.3 in which $\gamma=\alpha$ was set on an L-shaped domain, we choose $\alpha=2$ in this example, so that the resulting vector field is non-harmonic for $\gamma\neq\alpha$, and

$$\nabla\times\boldsymbol{u}=\left\langle 0,0,-\Delta\left(r^{\gamma}\sin\left(\alpha\theta\right)\right)\right\rangle=\left\langle 0,0,\left(\alpha^2-\gamma^2\right)\left(x^2+y^2\right)^{\gamma/2-1}\sin\left(\alpha\theta\right)\right\rangle.$$

Consequently, $\nabla\times\boldsymbol{u}\notin L^2(\Omega)$ if $\gamma\leq 1$. Nevertheless, due to the unique nature of the PDWG method, we still obtain noteworthy convergence result for the case of $\gamma\leq 1$. In Table 6, we have compiled several cases ranging from smooth to singular and plotted the PDWG approximation vs $\mathcal{Q}_h\boldsymbol{u}$ in Fig. 8.

- *Regular case* $\gamma=1.25$: $\mathbf{e}_{\boldsymbol{u}}$ and e_s show the optimal rates of convergence at $O(h)$, while $\mathbf{e}_{\mathcal{Q}_h\boldsymbol{u}}$ shows a superconvergence. $(e_\lambda,\mathbf{e}_q)$ only shows a slightly suboptimal rate of convergence during first two refinements, and optimal thereafter.

Table 6
Errors and the rates of convergence with different γ for Example 5.

	$1/h$	$\|\mathbf{e}_{\boldsymbol{u}}\|$	Rate	$\|\varepsilon^{1/2}\mathbf{e}_{\mathcal{Q}_h\boldsymbol{u}}\|$	Rate	$\|\|\|(e_\lambda, \mathbf{e}_{\boldsymbol{q}})\|\|\|$	Rate	$\|\|\|e_s\|\|\|$	Rate
$\gamma = 5/4$ (smooth)	2	3.96e-1	–	1.62e-1	–	9.01e-1	–	8.23e-2	–
	4	2.09e-1	0.92	7.69e-2	1.07	4.94e-1	0.87	5.12e-2	0.68
	8	1.07e-1	0.96	3.23e-2	1.25	2.63e-1	0.91	2.70e-2	0.93
	16	5.44e-2	0.98	1.26e-3	1.35	1.37e-1	0.94	1.32e-2	1.03
$\gamma = 1$ (singular)	2	5.34e-1	–	2.46e-1	–	1.20e0	–	1.42e-1	–
	4	3.06e-1	0.80	1.28e-1	0.94	7.11e-1	0.76	8.95e-2	0.66
	8	1.67e-1	0.87	5.58e-2	1.19	4.04e-1	0.81	4.94e-2	0.86
	16	8.82e-2	0.88	2.55e-2	1.13	2.25e-1	0.85	2.56e-2	0.95
$\gamma = 2/3$ (singular)	2	8.87e-1	–	4.55e-1	–	2.05e0	–	3.41e-1	–
	4	5.87e-1	0.59	2.75e-1	0.73	1.40e0	0.55	2.39e-1	0.51
	8	3.70e-1	0.67	1.39e-1	0.98	9.28e-1	0.60	1.53e-1	0.65
	16	2.34e-1	0.66	7.51e-2	0.89	6.01e-1	0.62	9.51e-2	0.68

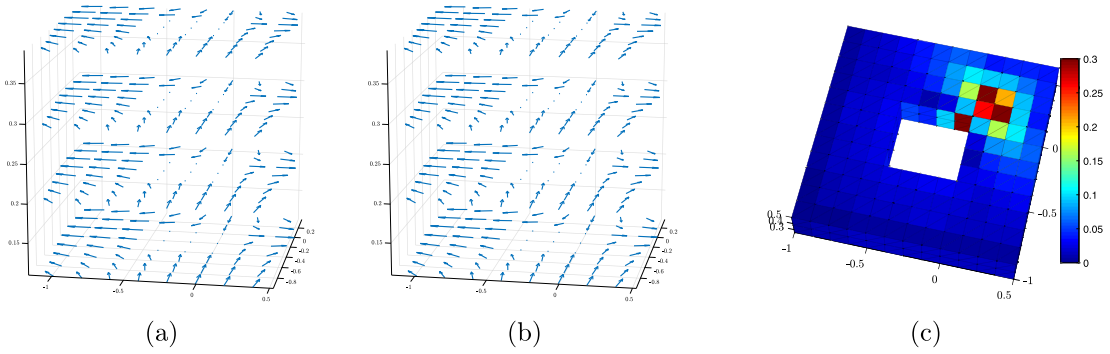

Fig. 8. Example 5: The vector field of $\mathcal{Q}_h\boldsymbol{u}$ is shown in (a) versus the PDWG approximation (b) for $\gamma = 2/3$ (singular case). The vector fields are plotted on several $z = c$ planes. The distribution of $\|\varepsilon^{1/2}\mathbf{e}_{\boldsymbol{u}}\|_T$ locally is plotted in (c) on the cut plane $z = 1/4$ with meshsize $h = 1/8$.

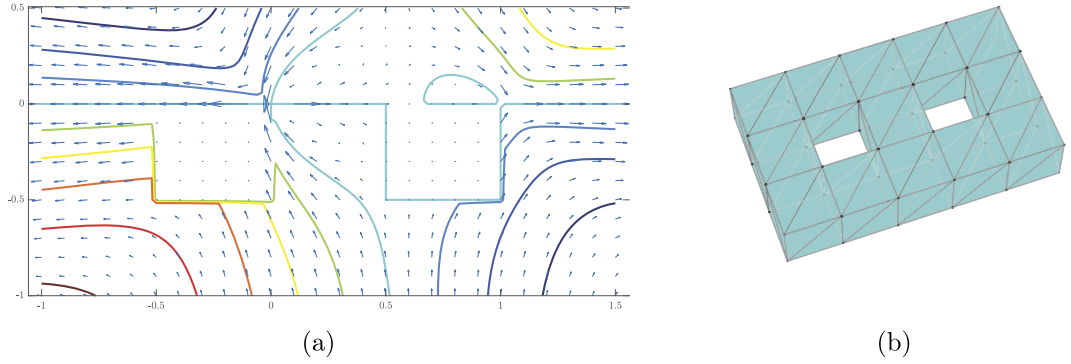

Fig. 9. Example 6: the singular true solution vector field when $\gamma_1 = 1/2$, $\gamma_2 = 2/3$, and $\alpha = 2$ is shown in (a) view from above on $z = 0$ plane. The level set contours are for the z-component of the vector potential used. The coarse mesh ($h = 1/2$) is illustrated in (b).

- *Singular case* $\gamma = 1$*:* In this case, we have $\boldsymbol{u} \in H^{1-\epsilon}_{loc}(\Omega)$ and $\boldsymbol{u} \notin \boldsymbol{H}(\mathbf{curl})$. $\mathbf{e}_{\boldsymbol{u}}$ shows a rate of convergence at $O(h^{0.9})$ asymptotically. Like the smooth case, $\mathbf{e}_{\mathcal{Q}_h\boldsymbol{u}}$ shows a superconvergence with rates higher than 1. $(e_\lambda, \mathbf{e}_{\boldsymbol{q}})$ and e_s show an optimal rate of convergence asymptotically.
- *Singular case* $\gamma = 2/3$*:* In this case, one has $\boldsymbol{u} \in H^{2/3-\epsilon}(\Omega)$, and $\boldsymbol{u} \notin \boldsymbol{H}(\mathbf{curl})$. Both $\mathbf{e}_{\boldsymbol{u}}$ and e_s show optimal rate of convergence at $O(h^{2/3})$. Similarly to previous two cases, $\mathbf{e}_{\mathcal{Q}_h\boldsymbol{u}}$ exhibits superconvergence with a rate of $O(h^{0.9})$. $(e_\lambda, \mathbf{e}_{\boldsymbol{q}})$ shows a convergence with a slightly suboptimal rate of $O(h^{0.6})$.

7.6. Example 6

In this example we consider a singular solution bearing the same form with that in Example 5 on a toroidal domain: $\Omega = \left[(-1, \frac{3}{2})^2 \backslash \{[-\frac{1}{2}, 0]^2 \cup [\frac{1}{2}, 1] \times [-\frac{1}{2}, 0]\}\right] \times [0, \frac{1}{2}]$

$$\boldsymbol{u} = \nabla \times \left\langle 0, 0, r_1^{\gamma_1} \sin(\alpha\theta_1) + r_2^{\gamma_2} \sin(\alpha\theta_2) \right\rangle,$$

where (r_i, θ_i) are the cylindrical coordinates centered at two different points; specifically, $r_1 = \sqrt{x^2 + y^2}$, $r_2 = \sqrt{(x-1)^2 + y^2}$, $\theta_1 = \arctan(y/x) + c_1$, and $\theta_2 = \arctan\left(y/(x-1)\right) + c_2$. In this example, we choose $\gamma_1 = 1/2$ and $\gamma_2 = 2/3$ such that the vector field is singular near the nonconvex corners of the domain (see Fig. 9). In fact, the vector field $\boldsymbol{u}$ behaves as $H^{1/2-\epsilon}$-regular in a neighborhood of the edge $\{x = 0, y = 0\}$, and as $H^{2/3-\epsilon}$-regular in a neighborhood of the edge $\{x = 1, y = 0\}$. In this example, one has $\boldsymbol{u} \notin \boldsymbol{H}(\mathbf{curl})$ as in Example 5. The convergence results are shown in Table 7. It can be seen that $\mathbf{e}_{\boldsymbol{u}}$, $(e_\lambda, \mathbf{e}_{\boldsymbol{q}})$, and e_s show optimal rates of convergence at $O(h^{1/2})$. The local error is more prominent near one of the nonconvex corners where $\boldsymbol{u}$ locally is $H^{1/2-\epsilon}$-regular (see Fig. 10). Similarly to previous two cases, $\mathbf{e}_{\mathcal{Q}_h\boldsymbol{u}}$ shows superconvergence with a rate approximately at $O(h^{3/4})$.

Table 7
Errors and the rates of convergence for Example 6.

	$1/h$	$\|\mathbf{e}_u\|$	Rate	$\|\varepsilon^{1/2}\mathbf{e}_{Q_h u}\|$	Rate	$\|\|\|(e_\lambda, \mathbf{e}_q)\|\|\|$	Rate	$\|\|\|e_s\|\|\|$	Rate
$\gamma_1 = 1/2$	2	1.49e0	–	8.37e-1	–	3.39e0	–	6.38e-1	–
$\gamma_2 = 2/3$	4	1.04e0	0.52	5.18e-1	0.69	2.48e0	0.45	4.74e-1	0.43
	8	6.99e-1	0.57	2.84e-1	0.87	1.77e0	0.49	3.27e-1	0.54
	16	4.79e-1	0.55	1.70e-1	0.73	1.24e0	0.51	2.22e-1	0.55

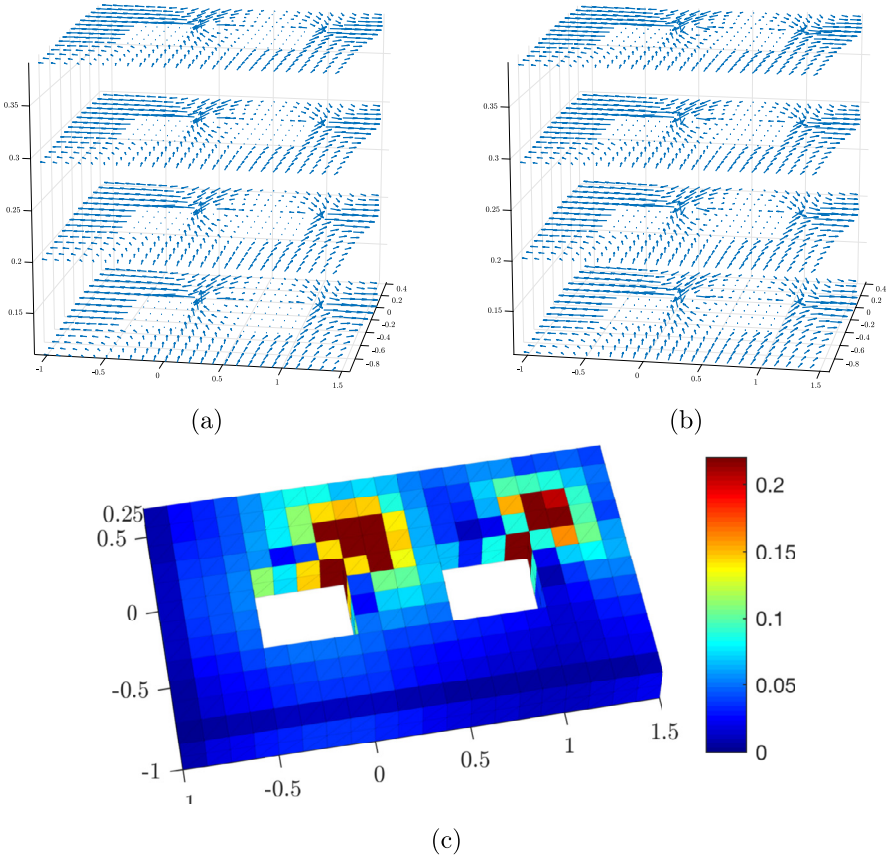

Fig. 10. Example 6: The vector field of $Q_h \boldsymbol{u}$ is shown in (a) versus the PDWG approximation (b) for $\gamma_1 = 1/2$ and $\gamma_2 = 2/3$ (singular case). The vector fields are plotted on several $z = c$ planes. The distribution of $\|\varepsilon^{1/2}\mathbf{e}_u\|_T$ locally is plotted in (c) on the cut plane $z = 1/4$ with meshsize $h = 1/8$.

Table 8
Errors and the rates of convergence with different β for Example 7.

	$1/h$	$\|\mathbf{e}_u\|$	Rate	$\|\varepsilon^{1/2}\mathbf{e}_{Q_h u}\|$	Rate	$\|\|\|(e_\lambda, \mathbf{e}_q)\|\|\|$	Rate	$\|\|\|e_s\|\|\|$	Rate
$\gamma = 2/3$	2	1.26e0	–	8.08e-1	–	2.52e0	–	3.68e-1	–
$\beta = 1$	4	8.78e-1	0.52	6.35e-1	0.35	1.63e0	0.63	2.54e-1	0.53
	8	6.71e-1	0.39	5.55e-1	0.19	1.03e0	0.66	1.58e-1	0.68
	16	5.82e-1	0.21	5.33e-1	0.06	6.44e-1	0.67	9.72e-2	0.70
$\gamma = 2/3$	2	3.42e0	–	2.75e0	–	5.32e0	–	6.52e-1	–
$\beta = 5$	4	2.89e0	0.25	2.66e0	0.05	3.16e0	0.75	4.05e-1	0.69
	8	2.71e0	0.09	2.64e0	0.01	1.79e0	0.82	2.21e-1	0.87
	16	2.66e0	0.03	2.64e0	0.00	1.01e0	0.82	1.27e-1	0.80

7.7. Example 7

In this example, we report some computational results for a test problem on a toroidal domain with first Betti number 1. As illustrated in Table 8, no convergence can be seen for the approximate solution $\boldsymbol{u}_h$, which is consistent with Theorem 6.2 due to the presence of a nontrivial harmonic vector field. The true solution is obtained by combining the ones used in Examples 1 and 5:

$$\boldsymbol{u}(x,y,z) = \nabla \times \left\langle 0, 0, r^\gamma \sin(\alpha\theta) \right\rangle + \beta \begin{pmatrix} \sin(\pi x)\cos(\pi y) \\ -\sin(\pi y)\cos(\pi x) \\ 0 \end{pmatrix}.$$

In this test, we choose $\alpha = 2$, $\gamma = 2/3$, such that $\boldsymbol{u} \in \boldsymbol{H}^{2/3-\epsilon}$, while the extra term with coefficient β is smooth thus not affecting the regularity of the solution. Observe that the extra β term is not divergence free. The optimal rate of convergence should be of order $O(h^{2/3})$ on simply-connected domains unaffected by the β term. As β varies, the numerical results do not demonstrate any convergence for the vector field $\boldsymbol{u}$, while optimal order of convergence is seen for both $(e_\lambda, \mathbf{e}_q)$ and e_s. The numerical performance is in consistency with our theory as established in Theorem 6.1 for the convergence of $(e_\lambda, \mathbf{e}_q)$ and e_s and Theorem 6.2 for the convergence of the vector field $\boldsymbol{u}_h$ up to a harmonic field. The vector fields of $Q_h \boldsymbol{u}$ and $\boldsymbol{u}_h$ are plotted in Fig. 11 (see (a) and (b)), while

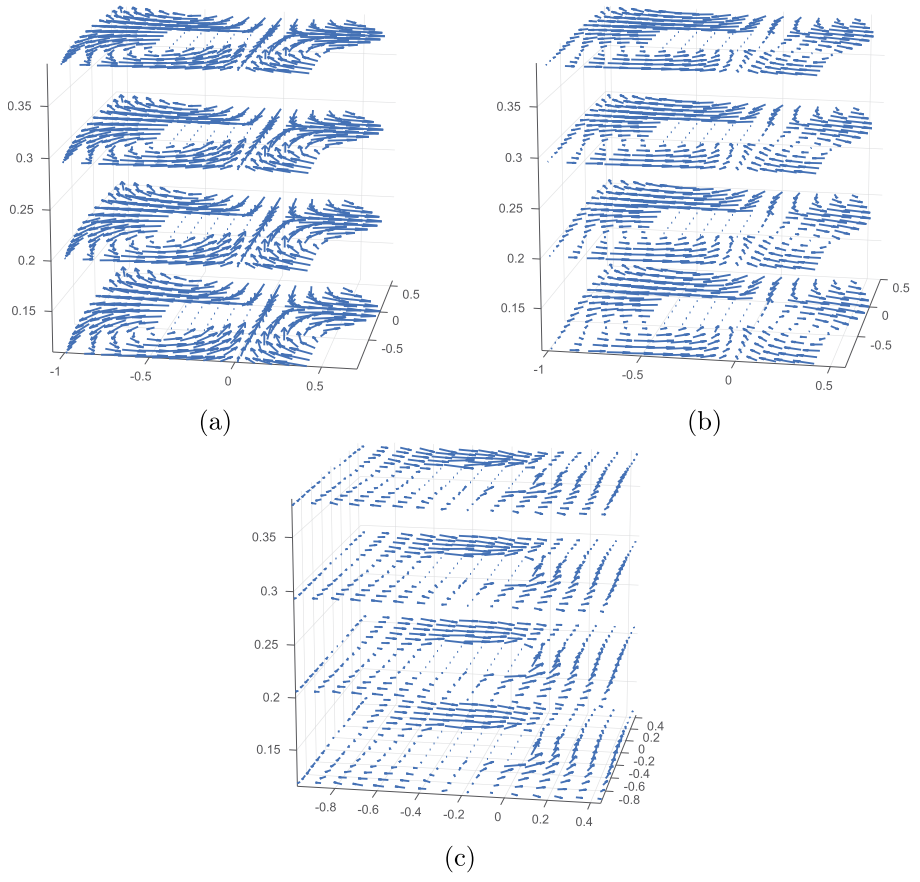

Fig. 11. Example 7: The vector fields of $\mathcal{Q}_h\boldsymbol{u}$ in (a) and that of the PDWG approximation (b) are visually different when $\boldsymbol{u}$ is not divergence-free on a toroidal domain. The discrete harmonic field $\boldsymbol{\eta}_h = \mathcal{Q}_h\boldsymbol{u} - \boldsymbol{u}_h$ is plotted in (c). The plots are on several $z = c$ planes.

their difference $\boldsymbol{\eta}_h = \mathcal{Q}_h\boldsymbol{u} - \boldsymbol{u}_h$ is plotted in the same figure as (c). According to Theorem 6.2, the vector field $\boldsymbol{\eta}_h$ is an approximate harmonic field with normal boundary condition.

Link to the Reproducible Capsule

https://doi.org/10.24433/CO.4347043.v1

Acknowledgement

We would like to express our gratitude to Dr. Long Chen (UCI) for his valuable discussion and suggestions.

Appendix A. Helmholtz decomposition

Theorem A.1. *For any vector-valued function $\boldsymbol{u} \in [L^2(\Omega)]^3$, there exists a unique $\boldsymbol{\psi} \in H_0(curl;\Omega)$, $\phi \in H^1(\Omega)/\mathbb{R}$, and $\boldsymbol{\eta} \in \mathbb{H}_{\varepsilon n,0}(\Omega)$ such that*

$$\boldsymbol{u} = \varepsilon^{-1}\nabla\times\boldsymbol{\psi} + \nabla\phi + \boldsymbol{\eta}, \tag{A.1}$$

$$\nabla\cdot(\varepsilon\boldsymbol{\psi}) = 0,\ \langle\varepsilon\boldsymbol{\psi}\cdot\boldsymbol{n}_i, 1\rangle_{\Gamma_i} = 0,\ i = 1,\dots,L. \tag{A.2}$$

Moreover, the following estimate holds true

$$\|\boldsymbol{\psi}\|_{H(\mathrm{curl};\Omega)} + \|\nabla\phi\|_0 \lesssim (\varepsilon\boldsymbol{u},\boldsymbol{u})^{\frac{1}{2}}. \tag{A.3}$$

Proof. The following is a sketch of the proof. Consider the problem of seeking $\boldsymbol{\psi} \in \mathbb{W}_\varepsilon(\Omega)$ such that

$$(\varepsilon^{-1}\nabla\times\boldsymbol{\psi}, \nabla\times\boldsymbol{\varphi}) = (\boldsymbol{u}, \nabla\times\boldsymbol{\varphi}), \quad \forall\,\boldsymbol{\varphi} \in \mathbb{W}_\varepsilon(\Omega). \tag{A.4}$$

Denote by

$$a(\boldsymbol{\psi},\boldsymbol{\varphi}) := (\varepsilon^{-1}\nabla\times\boldsymbol{\psi}, \nabla\times\boldsymbol{\varphi})$$

the bilinear form defined on $\mathbb{W}_\varepsilon(\Omega)$. We claim that $a(\cdot,\cdot)$ is coercive with respect to the $H(\mathrm{curl};\Omega)$-norm. To this end, it suffices to derive the following estimate

$$\|\boldsymbol{v}\|_0 \lesssim \|\nabla\times\boldsymbol{v}\|_0, \qquad \boldsymbol{v} \in \mathbb{W}_\varepsilon(\Omega). \tag{A.5}$$

In fact, for $\boldsymbol{v} \in \mathbb{W}_\varepsilon(\Omega)$, from Theorem 3.4 (Chapter 1) of [13], there exists a vector potential function $\boldsymbol{\omega} \in [H^1(\Omega)]^3$ such that

$$\varepsilon\boldsymbol{v} = \nabla\times\boldsymbol{\omega},\ \nabla\cdot\boldsymbol{\omega} = 0,\ \|\boldsymbol{\omega}\|_1 \lesssim (\varepsilon\boldsymbol{v},\boldsymbol{v})^{\frac{1}{2}}. \tag{A.6}$$

Using the integration by parts and the condition $\boldsymbol{v}\times\boldsymbol{n} = 0$ on Γ, we have

$$(\varepsilon\boldsymbol{v},\boldsymbol{v}) = (\nabla\times\boldsymbol{\omega},\boldsymbol{v}) = (\boldsymbol{\omega}, \nabla\times\boldsymbol{v}).$$

It follows from the Cauchy-Schwarz inequality and (A.6) that

$$(\varepsilon\boldsymbol{v},\boldsymbol{v}) \le \|\boldsymbol{\omega}\|_0\ \|\nabla\times\boldsymbol{v}\|_0 \lesssim (\varepsilon\boldsymbol{v},\boldsymbol{v})^{\frac{1}{2}}\ \|\nabla\times\boldsymbol{v}\|_0,$$

which implies (A.5).

Now from the Lax-Milgram Theorem, there exists a unique $\boldsymbol{\psi} \in \mathbb{W}_\varepsilon(\Omega)$ satisfying the equation (A.4) such that

$$\|\boldsymbol{\psi}\|_{H(\mathrm{curl};\Omega)} \lesssim (\varepsilon\boldsymbol{u},\boldsymbol{u}).$$

It is easy to see that $\mathbb{W}_\varepsilon(\Omega)$ is equivalent to the following quotient space:

$$H_0(\mathrm{curl};\Omega)/(\nabla H^1_{0c}(\Omega)) = \{\boldsymbol{v} \in H_0(\mathrm{curl};\Omega) :\ (\varepsilon\boldsymbol{v}, \nabla\phi) = 0,\ \forall\phi \in H^1_{0c}(\Omega)\}.$$

Thus, by using a Lagrangian multiplier $p \in H^1_{0c}(\Omega)$, the problem (A.4) can be re-formulated as follows: Find $\boldsymbol{\psi} \in H_0(\mathrm{curl};\Omega)$ and $p \in H^1_{0c}(\Omega)$ such that

$$\begin{aligned}(\varepsilon^{-1}\nabla\times\boldsymbol{\psi},\nabla\times\boldsymbol{\varphi})+(\varepsilon\nabla p,\boldsymbol{\varphi})&=(\boldsymbol{u},\nabla\times\boldsymbol{\varphi}),\quad &\forall\ \boldsymbol{\varphi}\in H_0(\mathrm{curl};\Omega),\\ (\boldsymbol{\psi},\varepsilon\nabla s)&=0,\quad &\forall\ s\in H^1_{0c}(\Omega).\end{aligned}\tag{A.7}$$

It follows from the first equation of (A.7) that

$$\nabla\times(\boldsymbol{u}-\varepsilon^{-1}\nabla\times\boldsymbol{\psi})-\varepsilon\nabla p=0.$$

Since $p\in H^1_{0c}(\Omega)$, the two terms on the left-hand side of the above equation are orthogonal in the ε^{-1}-weighted $L^2(\Omega)$ norm. Thus, we have

$$\nabla\times(\boldsymbol{u}-\varepsilon^{-1}\nabla\times\boldsymbol{\psi})=0,$$

which gives

$$\boldsymbol{u}-\varepsilon^{-1}\nabla\times\boldsymbol{\psi}\in H^0(\mathrm{curl};\Omega).$$

Thus, there exist unique $\phi\in H^1(\Omega)/\mathbb{R}$ and $\boldsymbol{\eta}\in\mathbb{H}_{\varepsilon n,0}(\Omega)$ such that

$$\boldsymbol{u}-\varepsilon^{-1}\nabla\times\boldsymbol{\psi}=\nabla\phi+\boldsymbol{\eta},$$

which completes the proof of the theorem. □

References

[1] R. Bensow, M.G. Larson, Discontinuous least-squares finite element method for the div-curl problem, Numer. Math. 101 (2005) 601–617.
[2] P.B. Bochev, K. Peterson, C.M. Siefert, Analysis and computation of compatible least-squares methods for div-curl equations, SIAM J. Numer. Anal. 49 (2011) 159–181.
[3] A. Bossavit, Computational Electromagnetism, Academic Press, San Diego, 1998.
[4] R. Brezzi, A. Buffa, Innovative mimetic discretizations for electromagnetic problems, J. Comput. Appl. Math. 234 (2010) 1980–1987.
[5] W. Cao, C. Wang, New primal-dual weak Galerkin finite element methods for convection-diffusion problems, arXiv:2001.06847.
[6] L. Chen, iFEM: an innovative finite element methods package in MATLAB, UC Irvine, https://urldefense.proofpoint.com/v2/url?u=https-3A_github.com_lyc102_ifem&d=DwIGaQ&c=sJ6xIWYx-zLMB3EPkvcnVg&r=QtnIF78hhsM9Up6dUV0D7t6Ch_FavnaE9me8zKe_FuA&m=d7WP5BWHVAEt_s-7qHQmcRwBQ4M1ORsvanPo24pT--A&s=1cVB2qyv-lViiqmYhKL6n3L8QZvOiFMJOF9MUnrCOyg&e=, 2009.
[7] P.G. Ciarlet, The Finite Element Method for Elliptic Problems, North-Holland, 1978.
[8] D.M. Copeland, J. Gopalakrishnan, J.E. Pasciak, A mixed method for axisymmetric div-curl systems, Math. Comput. 77 (2008) 1941–1965.
[9] S. Delcourte, K. Domelevo, P. Omnes, A discrete duality finite volume approach to Hodge decomposition and div–curl problems on almost arbitrary two-dimensional meshes, SIAM J. Numer. Anal. 45 (2007) 1142–1174.
[10] E. Burman, Error estimates for stabilized finite element methods applied to ill-posed problems, C. R. Acad. Sci. Paris, Ser. I 352 (2014) 655–659.
[11] E. Burman, Stabilized finite element methods for nonsymmetric, noncoercive, and ill-possed problems. Part I: elliptic equations, SIAM J. Sci. Comput. 35 (6) (2013) A2752–A2780.
[12] E. Burman, Stabilized finite element methods for nonsymmetric, noncoercive, and ill-possed problems. Part II: hyperbolic equations, SIAM J. Sci. Comput. 36 (4) (2014) A1911–A1936.
[13] V. Girault, P-A. Raviart, Finite Element Methods for Navier-Stokes Equations: Theory and Algorithms, Springer-Verlag Berlin Heidelberg, 1986.
[14] D. Li, C. Wang, J. Wang, Primal-dual weak Galerkin finite element methods for linear convection equations in non-divergence form, arXiv:1910.14073.
[15] J. Li, Y. Huang, Time-Domain Finite Element Methods for Maxwell's Equations in Metamaterials, Springer, 2013.
[16] J. Li, X. Ye, S. Zhang, A weak Galerkin least-squares finite element method for div-curl systems, J. Comput. Phys. 363 (2018) 79–86.
[17] K. Lipnikov, G. Manzini, F. Brezzi, A. Buffa, The mimetic finite difference method for the 3D magnetostatic field problems on polyhedral meshes, J. Comput. Phys. 230 (2011) 305–328.
[18] Y. Liu, J. Wang, A primal-dual weak Galerkin method for div-curl systems with low-regularity solutions, arXiv:2003.11795v2.
[19] R.A. Nicolaides, Direct discretization of planar div–curl problems, SIAM J. Numer. Anal. 29 (1992) 32–56.
[20] R. Nicolaides, X. Wu, Covolume solutions of three-dimensional div-curl equations, SIAM J. Numer. Anal. 34 (1997) 2195–2203.
[21] A.A. Rodriguez, E. Bertolazzi, R. Ghiloni, A. Valli, Construction of a finite element basis of the first de Rham cohomology group and numerical solution of 3D magnetostatic problems, SIAM J. Numer. Anal. 51 (4) (2013) 2380–2402.
[22] C. Wang, A new primal-dual weak Galerkin finite element method for ill-posed elliptic Cauchy problems, J. Comput. Appl. Math. (2019) (available online).
[23] C. Wang, J. Wang, Discretization of div-curl systems by weak Galerkin finite element methods on polyhedral partitions, J. Sci. Comput. 68 (2016) 1144–1171.
[24] C. Wang, J. Wang, A primal-dual finite element method for first-order transport problems, J. Comput. Phys. 417 (2020) 109571.
[25] C. Wang, J. Wang, A primal-dual weak Galerkin finite element method for second order elliptic equations in non-divergence form, Math. Comput. 87 (2018) 515–545.
[26] C. Wang, J. Wang, A primal-dual weak Galerkin finite element method for Fokker-Planck type equations, SIAM J. Numer. Anal. 58 (5) (2020) 2632–2661, arXiv:1704.05606.
[27] C. Wang, J. Wang, Primal-dual weak Galerkin finite element methods for elliptic Cauchy problems, Comput. Math. Appl. 79 (3) (2020) 746–763.
[28] C. Wang, L. Zikatanov, Low regularity primal-dual weak Galerkin finite element methods for convection-diffusion equations, arXiv:1901.06743.
[29] J. Wang, X. Ye, A weak Galerkin mixed finite element method for second-order elliptic problems, Math. Comput. 83 (2014) 2101–2126.